

## **Supplementary Materials**

Ocean Salinities Reveal Strong Global Water Cycle Intensification during 1950-2000

Paul J. Durack\*, Susan E. Wijffels and Richard J. Matear

\*To whom correspondence should be addressed. E-mail: pauldurack@llnl.gov

[www.sciencemag.org/cgi/content/full/336/6080/\[PAGE\]/DC1](http://www.sciencemag.org/cgi/content/full/336/6080/[PAGE]/DC1)

This PDF file includes:

Supplementary Text

Figs. S1 to S9

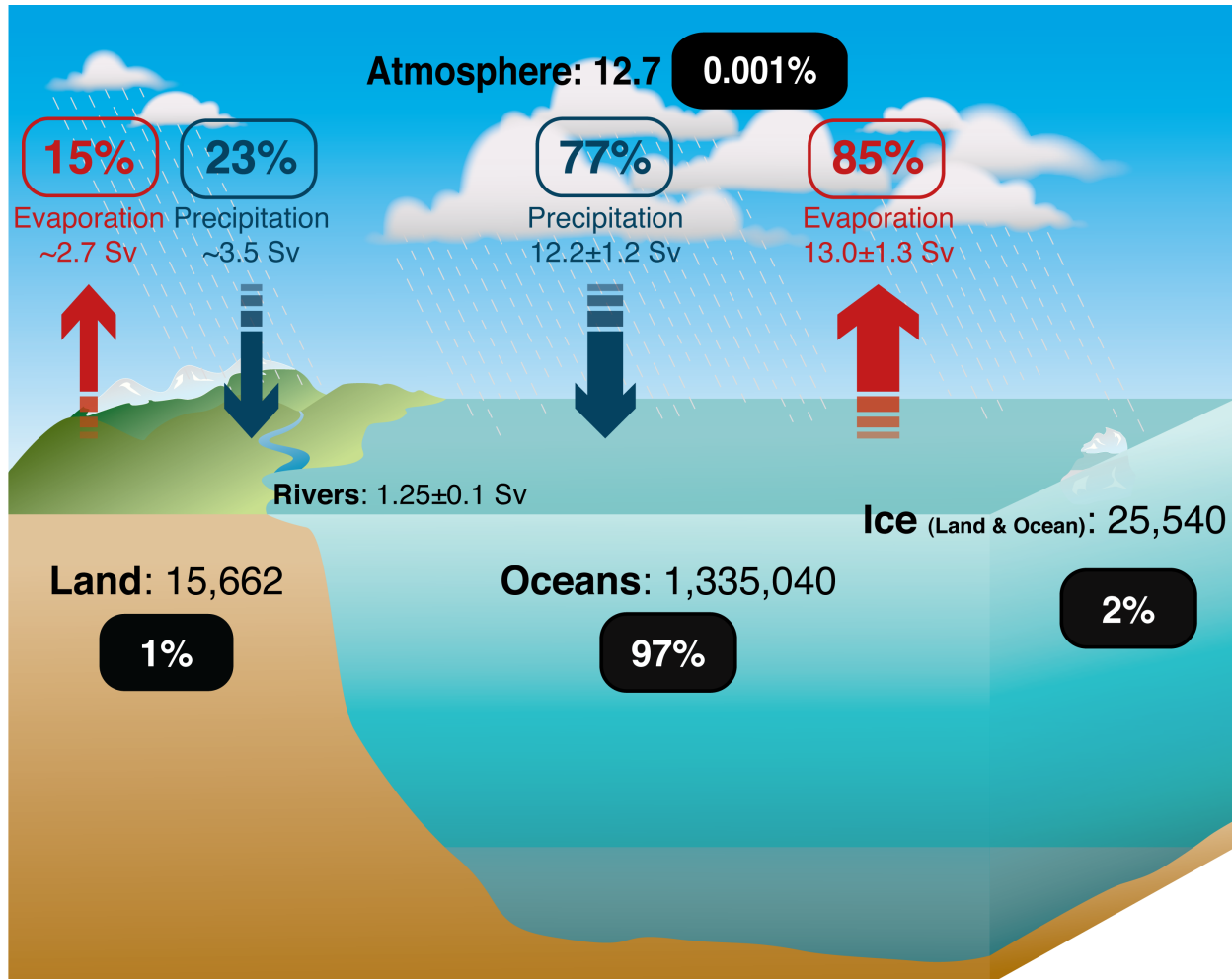
Tables S1 to S3

References (33-60)

04 August 2011; accepted 23 March 2012

DOI: 10.1126/science.1212222

## Supplementary Materials



Reservoirs represented by solid boxes:  $10^3 \text{ km}^3$ , fluxes represented by arrows: Sverdrups ( $10^6 \text{ m}^3 \text{ s}^{-1}$ )  
 Sources: Baumgartner & Reichel, 1975; Schmitt, 1995; Trenberth et al., 2007; Schanze et al., 2010; Steffen et al., 2010

Figure S1. Adapted schematic after (33, 34) and updated after (13, 35, 36) represents the key role of the ocean in the global water cycle – around 80% of the Earth's surface water fluxes occur at the ocean surface (rainfall: blue and evaporation: red unfilled boxes). Reservoir estimates represent storages in  $10^3 \text{ km}^3$ , flux estimates represent transports in Sverdrups ( $10^6 \text{ m}^3 \text{ s}^{-1}$ ) and values within boxes represent the approximate percentage of total storages (black filled boxes) or flux estimates (rainfall: blue; evaporation: red) for the global surface. Total ice volume expressed above is dominated by terrestrial sources, with sea-ice comprising approximately 0.1% of the ice storage total. Following (35) ice volumes are scaled with a 0.917 density factor to convert to liquid water equivalent.

## **1. Observational surface salinity change analysis**

For this analysis, new estimates of the surface salinity climatological annual mean and the 50 year (1950-2000) surface salinity change fields were obtained. This study used both the available quality-controlled historical hydrographic profiles, along with more recent data from the global Argo Program to determine long-term trends over the 50 year timescale (25).

The results presented in this analysis provide a broad-scale, globally consistent view of coherent, long-term global salinity changes which agree with many of the long-term regional salinity changes presented in many independent studies (22, 25 their Table 1). The key advantages of the new approach are its near global coverage (marginal seas and high-latitude seas >70° are excluded), and the methodology which is optimised to reduce biases due to seasonal and spatial sampling, particularly in the historical data, by fitting the mean climatology and trends concurrently. An attempt to remove biases associated with strong ENSO cycles is also an advantage of this analysis. In the sparsely historically observed Southern Hemisphere oceans, the analysis relies on Argo's ability to highly resolve the mean, seasonal and ENSO ocean responses. This methodology reduces aliasing by these observed phenomena into the multidecadal trend, with a 50 year temporal analysis long enough to account for many modes of cyclical climate variability. Due to the availability of ocean profile data, the varied temporal global sampling also means that any "simple" average represents different eras in different parts of the ocean (25 their Figure 2B, D), and by fitting the trend and mean climatology at the same time, errors due to a biased climatology are avoided.

Observed salinity change data can be downloaded from the CSIRO Ocean Change website at <http://www.cmar.csiro.au/oceanchange>.

### **1.1 Comparisons to previous observational surface salinity change estimates**

We selected two key global studies (24, 27) and provide quantified comparisons to directly compare the robustness of salinity pattern amplification magnitudes between these independent change estimates.

Each of these studies used different temporal periods for their analysis. An objective averaging methodology (24) generated pentads over the period 1955-1998 [which excludes the dominant modern footprint of Argo data, and was fundamental in the two comparable global studies (25, 27) and numerous recent regional analyses]. We have analysed this data and undertaken a linear regression for their full analysis grid to ascertain the spatial trend pattern for sea surface salinity (SSS). We then combine this with the World Ocean Atlas (2009) annual mean SSS climatology to develop the PA/PC metrics. The other global analysis (27) developed two temporal climatologies, a historical climatology that was centred around 1974 (pre-Argo) and another using just the modern Argo data (2003-2007), centred around 2005. They difference these climatologies to obtain the salinity change for 1974-2005. We then combine this with their estimate of the annual mean SSS climatology (based off historical data from World Ocean Database 2005, 1960-1989) to develop the PA/PC metrics.

The observed analysis (25) used in this study allows a direct calculation of 1950-2008 (scaled to represent 1950-2000; 50 year) changes, however the spatial footprint of the analysis is varied due to this methodology having to increase its search radius in order to sample across decadal “bins” from 1950-2010. In comparison (27) has a fixed spatial footprint, but varied temporal epochs, which leads to a temporally varying trend due to the sparsity of historical data [rather than spatially varying (25)]. Temporally averaged pentads are a feature of (24), which ensures a sound temporal analysis, however this analysis returns a zero estimate in regions of data sparsity and leads to patchy, noisy and difficult to interpret spatial patterns. At the time of this (24) analysis the Argo platform was in its infancy (and their analysis omitted the Argo period concluding in 1998), which has provided a solid baseline for near complete seasonal coverage of the global ocean in numerous subsequent studies. Additionally, these analyses (24, 27) did not attempt to resolve the mean spatial structure, or resolve and de-bias the data for seasonal coverage (particularly the Southern Hemisphere) and ENSO cycles, and noisier, less spatially coherent patterns were the result. For this reason while spatially varying the analysis used in this study (25) provides a more robust measure of the absolute temporal trend.

It is clear from an analysis of basin zonal mean SSS changes (not shown) that many of the broad-scale features presented in each of these studies are robust to the data used and the method of analysis. The broad-scale features of enhanced salinities in the Southern subtropics are apparent, and the freshening of the region under the ITCZ is also clear in a global zonal analysis for all 3 independent studies. A broad-scale freshening (dominated by the North Pacific Basin) is also apparent above 20N for all analyses.

In order to quantitatively compare the surface salinity results it was necessary to form basin zonal means for both climatological mean surface salinity and the surface trend fields for the representative studies. In the case of (24) their data is freely downloadable from the NODC website. For (27) their data was requested and provided to complete this analysis. Linear trends for the 43 year period (24) and 31 year period (27) were scaled to represent results directly comparable to the presented 50 year trends (25). Figure S2 captures the basin zonal mean results for each study.

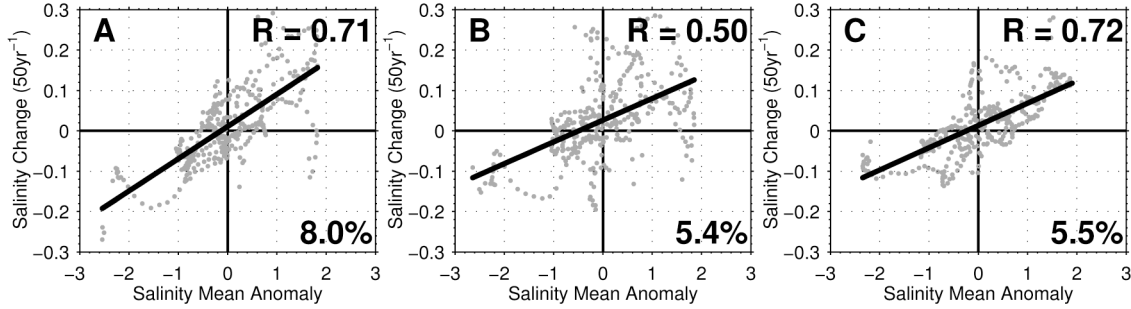


Figure S2. Basin zonal mean surface salinity comparison for the analyses of (A)(25), (B)(24) and (C)(27)

A linear relationship is evident in each analysis suggesting fresh waters are getting fresher and salty waters are getting saltier. Increased noise is apparent in (24) result with greater scatter and a lower pattern correlation (PC) value of  $\sim 0.5$  (Figure S2B). For (25) and the (27) results a higher pattern correlation (PC) value of  $\sim 0.7$  is apparent, suggesting a more spatially coherent result, with the change field more closely matching the climatological mean pattern.

Magnitudes of PA are more variable, with the (25) estimate (A) suggesting 8% (Figure S2A), whereas both results from (24) and (27) suggest a 50 year value of around  $\sim 5\%$ .

When comparing global zonal mean results (not shown; a less rigorous test, as this integrates across the salinity gradients for each basin which are present at differing latitudes. The basin zonal mean analysis depends upon these features to obtain the PA estimate), it would appear the (25) result does not systematically overestimate the SSS PA with the median PA of 5.2% (PC = 0.69) compared to 6.6% (PC = 0.71) and 2.8% (PC = 0.40) for (24) and (27) respectively. It is clear from the additional analysis presented in the following section 2.1 that basin zonal, or global zonal smoothing does tend to enhance the PC values in models and observations (compare Figure 2, J, K and L and Figure S4, A, B and C).

As previously described in detail by (25 their Table 1) many salinity change estimates exist, and the global and regional results presented by this analysis tend to agree with the broad-scale conclusions of previous estimates of regional and global estimates of surface and subsurface salinity change.

## 2. CMIP3: Model drift correction

Model (or climate) drift is an inherent problem in current state-of-the-art climate modelling systems (37). Drift is the term applied to a systematic bias in model fields, which can be attributed to deficiencies in the modelling system, with this feature primarily a problem with ocean simulations. These manifest due to many different reasons, primarily on two timescales. Rapid drift occurs and is most likely due to errors introduced when coupling the ocean and atmosphere model subcomponents, and is referred to as “coupling shock”. Longer term drift can be attributed to the slow adjustment of the modelled deep ocean, and the most likely causes of this drift can be linked to unresolved/sub-grid scale physics (exclusion of eddies, localised boundary flows), poor initialisation (deficiencies with “first/best guess” climatologies),

imposed flux adjustments (mostly deprecated in CMIP3) and insufficient model “spin-up” (incomplete initialisation of the coupled model, so that a pseudo-equilibrium climate state in the model is never reached).

In order to effectively obtain the most accurate estimate of the transient greenhouse gas (GHG) forced signal from a climate model simulation, and in particular the low signal-to-noise externally forced 20C3M simulations, it is necessary to attempt to account for drift. It is also necessary to attempt to account for high and low-frequency variability, which can influence resolved trends. For this reason multidecadal trends over 50 years (1950-2000) are considered in this analysis, with an expectation that modelled climate variability will be fairly small over 50 year timescales when compared to the transient GHG-forced response (see following section CMIP3: Assessment of Modelled Internal Variability and Figure S4).

For the analysis presented here, drift was determined from the 1900-2049 period associated with the initial (run1: 1950-2000) 20C3M simulation, and the spatial pattern and magnitude was then removed from all the transient 20C3M simulations for each representative simulation. A test was undertaken to ensure that the differences in the time of 20C3M initialisation of the corresponding PICNTRL did not largely affect the result, and this was found to be a sound assumption, with the exception of the gfdl\_cm2\_0 run1. However as salinity was only available for run1 (and not the subsequent run2 or run3) for this model it didn't affect the analysis. The 1900-2049 period was selected as it bounded 1950-2000 (50 years either side), the period over which trends were obtained from 20C3M simulations and directly compared to the new observed estimates for the same period. Additionally, use of this early period ensured a larger ensemble of CMIP3 data was available, as available PICNTRL runs tend not to extend beyond 2100.

To test the sensitivity to this method of drift removal, a duplicated analysis was undertaken using the 2000-2149 periods, which bound 2050-2099 (the period of analysis for SRES simulations). These 2000-2149 drift estimates were then used to account for the drift in the available SRES simulations. A decrease in the total number of simulations available for this analysis was found, due to a reduction in available concurrent PICNTRL data (fewer models provide PICNTRL data that extends beyond 2100; Figure S3 versus Figure 2), however they key results expressed in Figure 2 are largely reproduced in this adapted analysis (Figure S3).

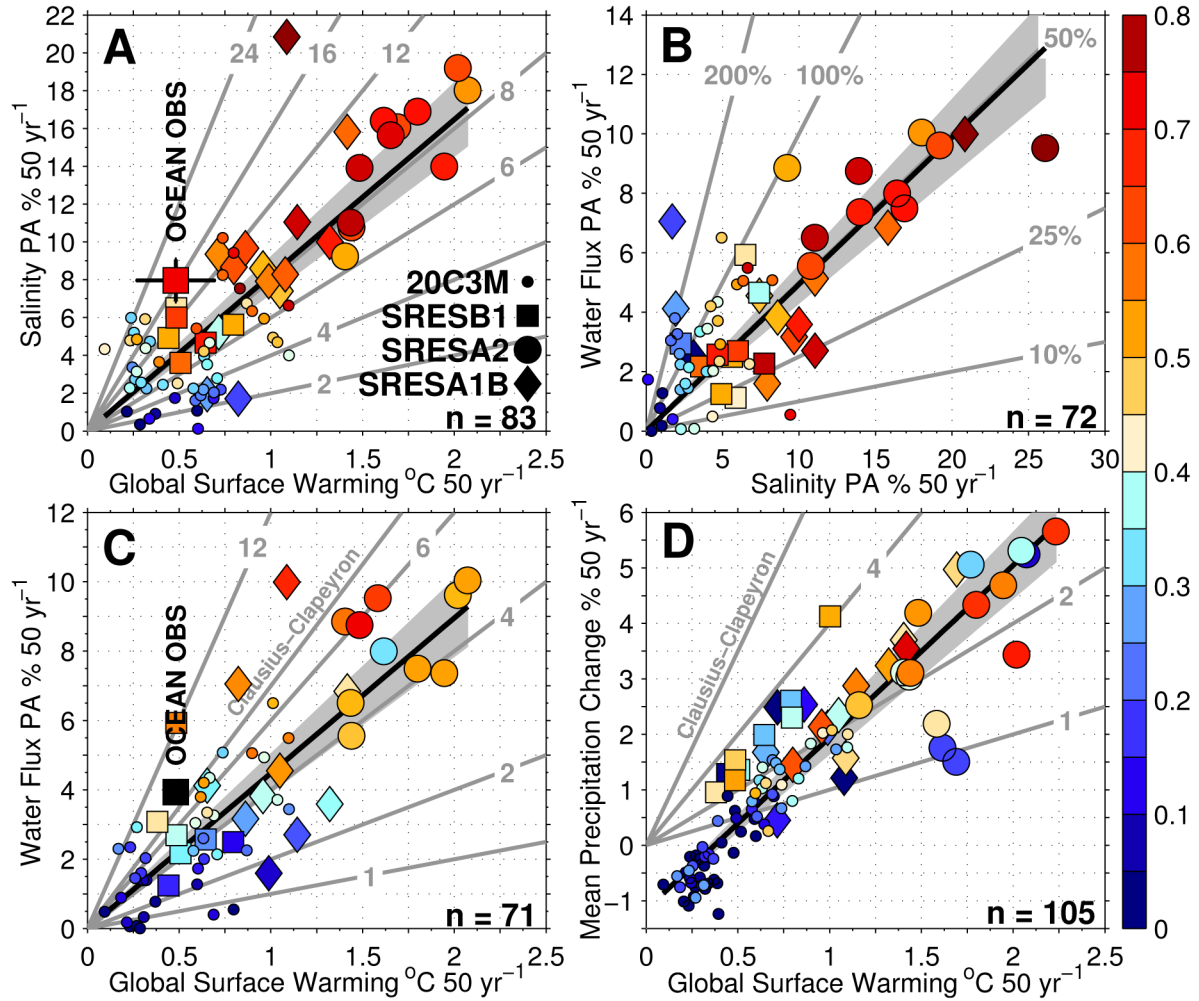


Figure S3. Representative change responses from the available CMIP3 simulations compared to new observational estimates of ocean salinity changes. Following Figure 2, however all SRES fields have been de-drifted using an appropriate pre-industrial control simulation for the period 2000–2149, rather than 1900–2049 (Fig. 2). The number of individual simulations which have been analysed for each variable is noted in the bottom right hand corner of each panel. (A) The surface salinity pattern amplification (PA; y axis) versus the corresponding global average surface temperature change ( $\Delta Ta$ ; x axis), colors are the salinity pattern correlation (PC). (B) Water flux (E-P; y axis) PA versus surface salinity PA (x axis), colors are the salinity PC. (C) Water flux (E-P; y axis) PA versus global  $\Delta Ta$  (x axis), colors are the E-P pattern correlation (PC). (D) Global spatial average precipitation change, rather than pattern amplification ( $\Delta P$ ; y-axis) versus global  $\Delta Ta$  (x axis), colors are the precipitation PC. Gray lines express constant proportional change. Gray shading [99% confidence interval (C.I.)] bounds the correlation-weighted linear best fit to the model ensemble for a line intersecting 0 (y axis; A, B, C) and -1.2 (y axis; D) in black. The 20th century (20C3M; 1950–2000) simulations are presented in small circles, and the three 21st century projected scenarios (SRES; 2050–2099) are shown as squares for B1, large circles for A2 and diamonds for A1B. Observational estimates are shown using a  $\Delta Ta$  value from HadCRUT3 in (A) PA from this study as the red square with black error bars showing the 99% C.I., and in (C) as the black square with the CMIP3-scaled result based from (A) (see text)

## **2.1 CMIP3: Assessment of Modelled Internal Variability**

To further test whether modelled variability has influenced the CMIP3 results an additional analysis was undertaken to compare the 50 year (1950-2000; 20C3M) analysed results to change patterns obtained over the full length ( $\sim$ 150 years) of the simulations expressed in Figure 1. As observational data coverage is only available for 1950-onwards, a directly comparable sensitivity analysis is not possible for the observational estimates. However, investigating modelled variability is insightful when considering what is cyclical versus transient change. Surface salinity patterns were assessed for their full temporal surface salinity trends, so 1850-2000 for the cccma\_cgcm3\_1\_t63 and 1860-2000 for ukmo\_hadgem1, to investigate the effects of modelled variability.

The observed result presented in Figure 1J is reproduced below (Figure S4A), however to further enhance variability the full spatial analysis is considered, rather than the zonal ocean basin averages presented in Figures 1 and 2. When comparing the results from this full grid analysis (Figure S4A) to the zonal mean analysis (Figure 1J) it is clear that spatial smoothing has enhanced the pattern correlation (PC; 0.5 – Figure S4A versus 0.7 Figure 1J). However, the surface salinity pattern amplification (PA) is approximately equivalent for each of the analyses; 7.7% (Figure S4A) compared to 8% (Figure 1J). Model analyses for 50 years are presented in Figure S4B, C and  $\sim$ 150 years in Figure S4, D and E respectively. Considering the cccma\_cgcm3\_1\_t63 model and the 50 year analysis, a slight increase in PC is also apparent due to the spatial smoothing (0.7 Figure 1K versus 0.6 Figure S4B), however reported PA is 6.1% for both the 50 year (Figure S4B) and  $\sim$ 150 year analysis (Figure S4D), with a decrease in PC for the  $\sim$ 150 years (0.6 versus 0.5). For ukmo\_hadgem1 similar results are found, with similar PA values recorded across all analyses (1.0% Figure 1L versus 0.6% and 0.4% Figure S4, C and E) and correspondingly low PC. This additional analysis supports the use of the 50 year periods used in this study, as these 50 year periods are truly representative of the full 20<sup>th</sup> century simulated change (Figure S4).

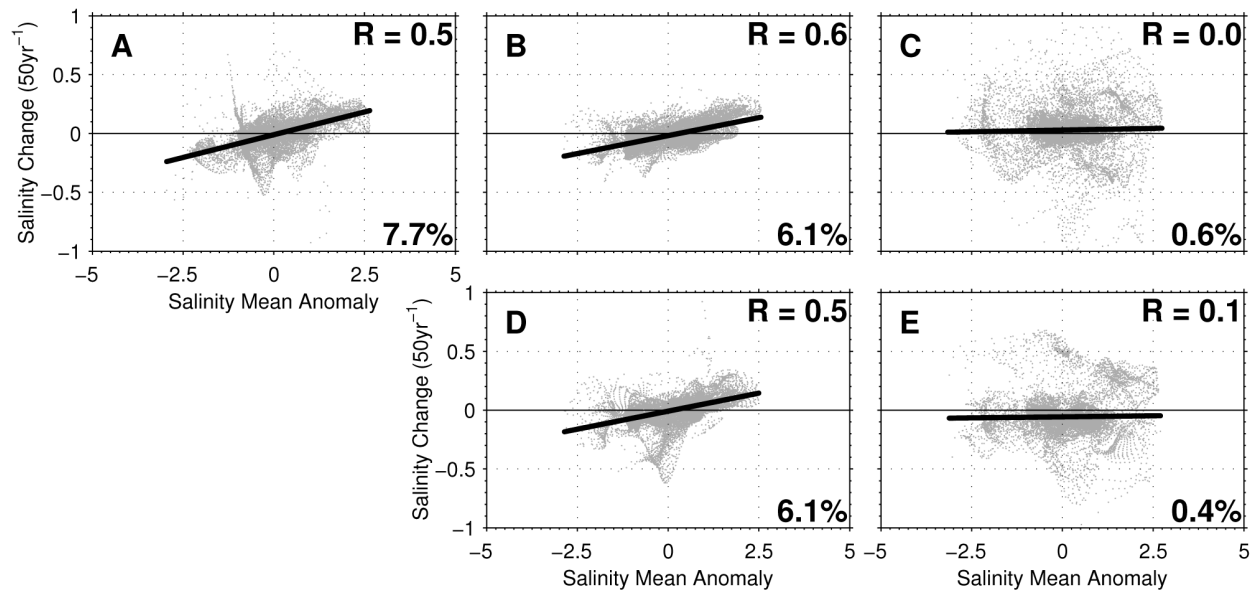


Figure S4. Examples of pattern amplification for global ocean surface salinity – values are plotted point-wise for the analysed surface response. Unlike Figure 1, fields are not spatially smoothed using the basin zonal mean approach. for (A) the 1950-2000 observed result (B) Canadian Centre for Climate Modelling & Analysis: CGCM3.1 (T63) for 1950-2000 (C) United Kingdom MetOffice: HadGEM1 for 1950-2000 (D) Canadian Centre for Climate Modelling & Analysis: CGCM3.1 (T63) for 1850-2000 (E) United Kingdom MetOffice: HadGEM1 for 1860-2000

## 2.2 CMIP3: The Role of Aerosols and other Forcing Agents

The effect of comprehensive aerosol schemes is known to provide a general cooling effect and a corresponding dampening effect on local water cycle operation (9, 10, 38). In CMIP3 20C3M simulations which incorporate volcanic aerosols forcing also generally include other aerosol effects such as black and organic carbon and sulphates (Table S1).

Table S1. Forcings and flux corrections used in CMIP3 simulations of 20<sup>th</sup> century climate change [Updated from (39)]. The letter 'Y' denotes inclusion of the specific forcing for the selected model. G: well-mixed greenhouse gases; O: tropospheric and stratospheric ozone; SD: sulphate aerosol direct effects; SI: sulphate aerosol indirect effects; BC: black carbon; OC: organic carbon; MD: mineral dust; SS: sea salt; LU: land use change; SO: solar irradiance; VL: volcanic aerosols. For flux corrections (FC) the following notation is used; Freshwater: F; Heat/momentum: H.

| Model              | Representative numbers     | G | O | SD | SI | BC | OC | MD | SS | LU | SO | VL | FC  |
|--------------------|----------------------------|---|---|----|----|----|----|----|----|----|----|----|-----|
| bccr_bcm2.0        | 1                          | Y | - | Y  | -  | -  | -  | -  | -  | -  | -  | -  | -   |
| cccmca_cgcm3_1_t47 | 2,3,4,5,6                  | Y | - | Y  | -  | -  | -  | -  | -  | -  | -  | -  | F,H |
| cccmca_cgcm3_1_t63 | 7                          | Y | - | Y  | -  | -  | -  | -  | -  | -  | -  | -  | F,H |
| cnrm_cm3           | 8                          | Y | Y | Y  | -  | Y  | -  | -  | -  | -  | -  | -  | -   |
| csiro_mk3_0        | 9,10,11                    | Y | Y | Y  | -  | -  | -  | -  | -  | -  | -  | -  | -   |
| csiro_mk3_5        | 12,13,14                   | Y | Y | Y  | -  | -  | -  | -  | -  | -  | -  | -  | -   |
| gfdl_cm2_0         | 15                         | Y | Y | Y  | -  | Y  | Y  | -  | -  | Y  | Y  | Y  | -   |
| gfdl_cm2_1         | 16                         | Y | Y | Y  | -  | Y  | Y  | -  | -  | Y  | Y  | Y  | -   |
| giiss_aom          | 17,18                      | Y | - | Y  | -  | -  | -  | -  | Y  | -  | -  | -  | -   |
| giiss_model_e_h    | 19,20,21,22,23             | Y | Y | Y  | Y  | Y  | Y  | Y  | Y  | Y  | Y  | Y  | -   |
| giiss_model_e_r    | 24,25,26,27,28,29,30,31,32 | Y | Y | Y  | Y  | Y  | Y  | Y  | Y  | Y  | Y  | Y  | -   |
| iap_fgoals1_0      | 33,34,35                   | Y | - | Y  | -  | -  | -  | -  | -  | -  | -  | -  | -   |
| invv_echam4        | 36                         | Y | Y | Y  | -  | -  | -  | -  | -  | -  | -  | -  | -   |
| ipsl_cm4           | 37                         | Y | - | Y  | Y  | -  | -  | -  | -  | -  | -  | -  | -   |
| miroc3_2_hires     | 38                         | Y | Y | Y  | Y  | Y  | Y  | Y  | Y  | Y  | Y  | Y  | -   |
| miroc_3_2_medres   | 39                         | Y | Y | Y  | Y  | Y  | Y  | Y  | Y  | Y  | Y  | Y  | -   |
| miuib_echo_g       | 40,41,42                   | Y | - | Y  | Y  | -  | -  | -  | -  | -  | Y  | Y  | F,H |
| mpi_echam5         | 43,44,45                   | Y | Y | Y  | Y  | -  | -  | -  | -  | -  | -  | -  | -   |
| mri_cgcm2_3_2a     | 46,47,48,49,50             | Y | - | Y  | -  | -  | -  | -  | -  | -  | Y  | Y  | F,H |
| ncar_ccsm3_0       | 51,52                      | Y | Y | Y  | -  | Y  | Y  | -  | -  | -  | Y  | Y  |     |
| ncar_pcm1          | 53,54,55                   | Y | Y | Y  | -  | -  | -  | -  | -  | -  | Y  | Y  |     |
| ukmo_hadcm3        | 56,57                      | Y | Y | Y  | Y  | -  | -  | -  | -  | -  | Y  | -  |     |
| ukmo_hadgem1       | 58                         | Y | Y | Y  | Y  | Y  | Y  | -  | -  | Y  | Y  | -  |     |

So how do aerosols affect the reported water cycle changes as expressed in sea surface salinity (SSS), surface water flux (E-P) pattern amplification (PA) and corresponding pattern correlations (PC)? The results presented in Figure 2 included all available simulation results from the 20C3M as well as the available SRES (A1B, A2 and B1) simulations. As volcanic aerosol emissions are not readily predictable into the future, these forcing agents were excluded from SRES simulations, however have been included in around half of the available 20C3M simulations (Table S1).

Representative change responses for many aspects of water cycle operation were presented in Figure 2. To focus on aerosol effects, Figure S5 reproduces the results presented in Figure 2A, B just for the 20C3M simulations. This sub-suite of simulations can then be assessed on whether they included volcanic aerosol effects, or whether they didn't (Table S1).

There appears to be a clear pattern of enhanced global surface warming in non-volcanic models (Figure S5A; contrast circles versus diamonds), with corresponding larger PA (Figure S5A colors) when compared to the volcanically-forced simulations. A clear pattern of low-warming simulations with low PA (Figure S5A; left-bottom), compared to high-warming simulations with comparatively higher PA (Figure S5A; right-top) is apparent. This tends to suggest that a clear signal-to-noise process is in operation, with a more coherent salinity PA response expressed in the stronger warming simulations, whereas many of the low-warming simulations show no such coherent salinity PA. When comparing the PA of both surface salinity and surface water flux (Figure S5B) this clear split appears even more prominently, with low salinity PA simulations also having low water flux PA (Figure S5B; left-bottom) and simulations with comparatively high salinity PA also having high surface water flux PA. A clear increase in PA is apparent (Figure S5B; colors – blue to red) from the lower left (noise) to the upper right (signal), with simulations with large PA values tending to be those which report a larger warming (Figure S5A).

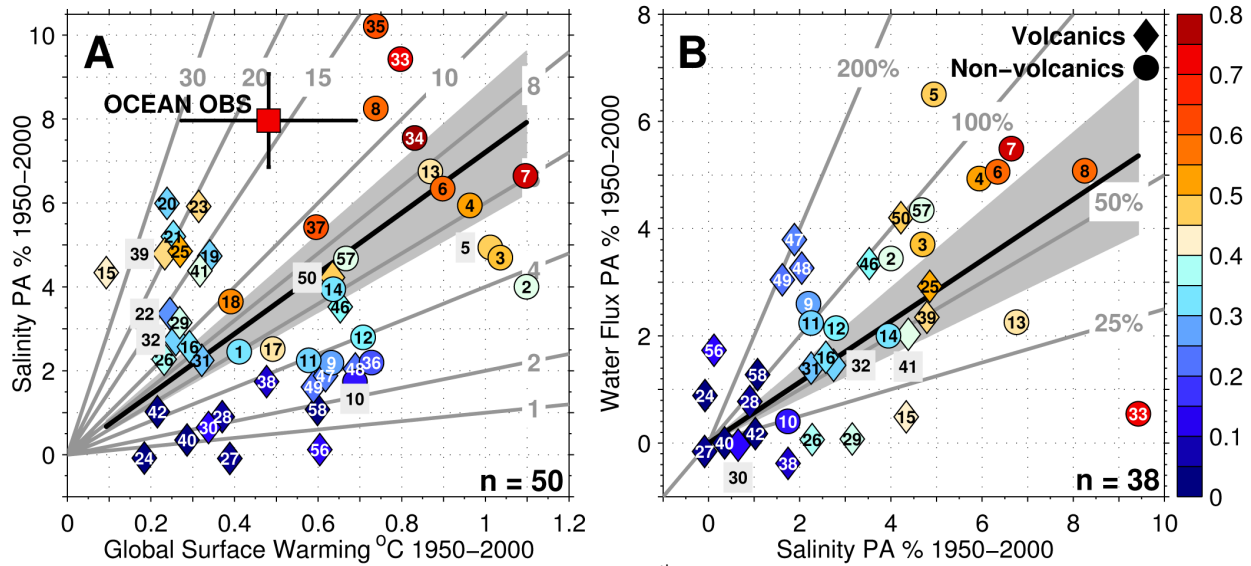


Figure S5. Pattern amplification (PA) rates for all available 20<sup>th</sup> century (20C3M; 1950–2000) de-drifted CMIP3 simulations. Diamonds represent 20C3M simulations which include volcanic aerosol forcing, circles are simulations without volcanic aerosol forcing. The number of individual simulations which have been analysed for each variable is noted in the bottom right hand corner of each panel. For (A) Surface salinity (y axis) versus the corresponding global average surface temperature change ( $\Delta Ta$ ; x axis). (B) Water flux PA (E-P; y axis) versus surface salinity PA (x axis). Colors are the salinity pattern correlation (PC) for both panels (A) and (B). Gray lines express constant proportional change. Gray shading (99% C.I.) bounds the correlation-weighted linear best fit to the model ensemble for a line intersecting 0 in black. Observational estimates are shown using a  $\Delta Ta$  value from HadCRUT3 in (A) PA from this study as the red square with black error bars showing the 99% confidence interval (C.I.). Numbers indicated in the figure align with the models and realisations expressed in Table S1 and S2.

The full ranges of CMIP3 20C3M change responses for 1950-2000 are contained in Table S2. These results include global change estimates for the 5 variables analysed, including; salinity and water flux (E-P) pattern amplification, ocean and global surface temperature and global mean rainfall changes ( $\Delta P$ ). For reference a comparative non-exhaustive selection of observed estimates from available data products is also included in the lower section of Table S2. The range of surface salinity responses, and spatial patterns of the associated drift estimates (see section above), along with 1950-2000 climatological surface salinity and water flux (E-P) means are contained in Figure S6.

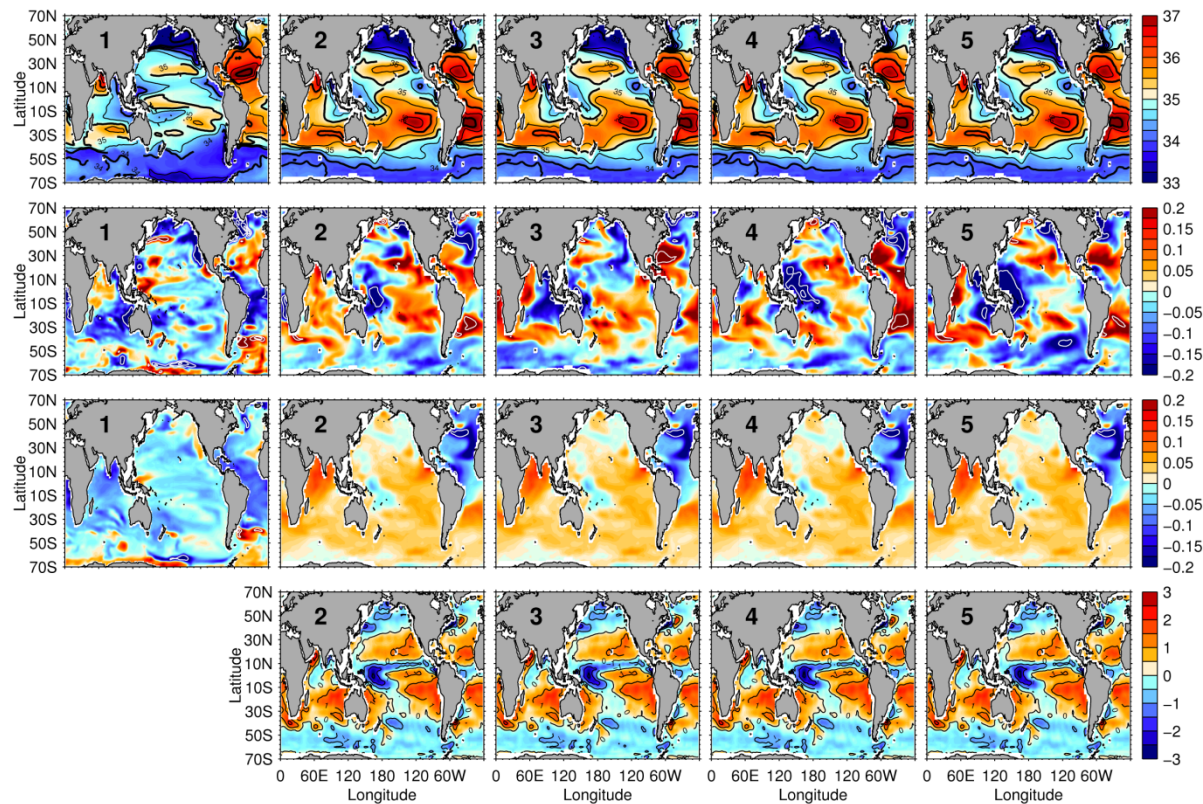
Table S2. Integrated global surface values for 1950-2000 trends resolved from available 20<sup>th</sup> century (20C3M) CMIP3 experiments, de-drifted by their corresponding pre-industrial control in: sea surface salinity (basin zonal-mean) pattern amplification (PA; %), ocean water flux (E-P) (basin zonal-mean) pattern amplification (PA; %), area-weighted global ocean surface temperature (°C), area-weighted global surface temperature (°C) and area-weighted global surface mean precipitation change (%). A non-exhaustive selection of observational estimates from available data products are found in the lower section of the table for comparison. Trends have been obtained over the period in parentheses and scaled to represent directly comparable 50 year changes.

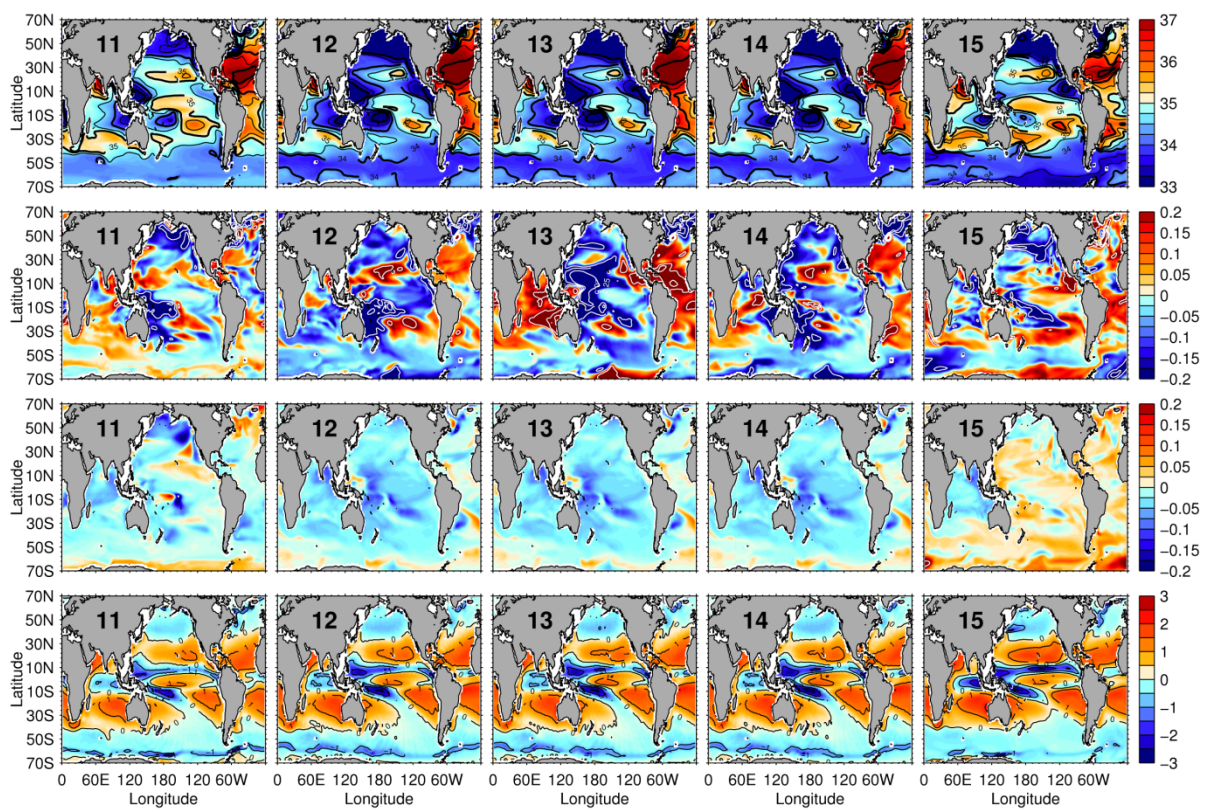
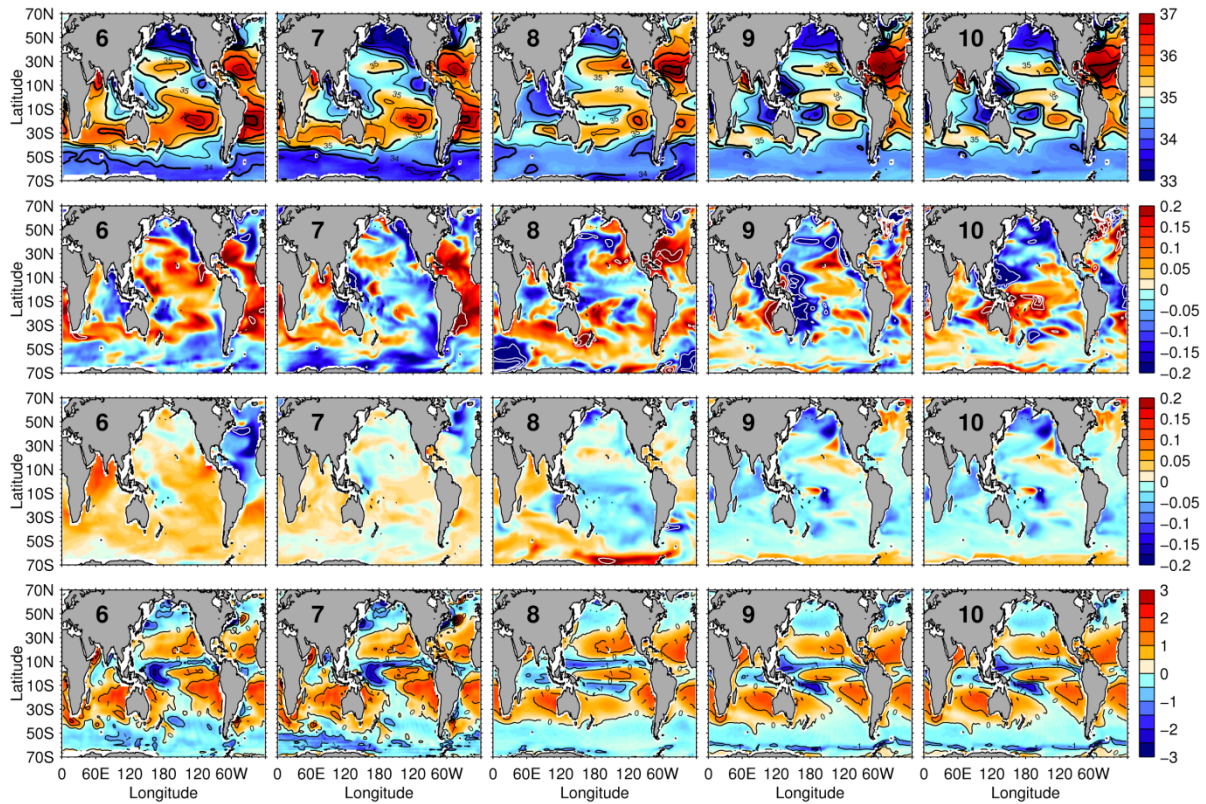
| #  | Model                         | Salinity<br>(%PA) | E-P<br>(%PA) | Ocean<br>Temperature<br>(°C) | Global<br>Temperature<br>(°C) | Rainfall<br>( $\Delta P$ ) |
|----|-------------------------------|-------------------|--------------|------------------------------|-------------------------------|----------------------------|
| 1  | bccr_bcm2_0.20c3m.run1        | +2.5              | -            | -                            | +0.41                         | +0.1                       |
| 2  | cccmma_cgcm3_1_t47.20c3m.run1 | +4.0              | +3.4         | +0.73                        | +1.10                         | +2.0                       |
| 3  | cccmma_cgcm3_1_t47.20c3m.run2 | +4.7              | +3.7         | +0.66                        | +1.04                         | +1.7                       |
| 4  | cccmma_cgcm3_1_t47.20c3m.run3 | +5.9              | +4.9         | +0.66                        | +0.96                         | +2.0                       |
| 5  | cccmma_cgcm3_1_t47.20c3m.run4 | +4.9              | +6.5         | +0.67                        | +1.01                         | +2.1                       |
| 6  | cccmma_cgcm3_1_t47.20c3m.run5 | +6.3              | +5.1         | +0.61                        | +0.90                         | +1.8                       |
| 7  | cccmma_cgcm3_1_t63.20c3m.run1 | +6.6              | +5.5         | +0.74                        | +1.10                         | +1.8                       |
| 8  | cnrm_cm3.20c3m.run1           | +8.3              | +5.1         | -                            | +0.74                         | +1.1                       |
| 9  | csiro_mk3_0.20c3m.run1        | +2.2              | +2.6         | +0.42                        | +0.63                         | +1.0                       |
| 10 | csiro_mk3_0.20c3m.run2        | +1.7              | +0.4         | +0.45                        | +0.69                         | +0.9                       |
| 11 | csiro_mk3_0.20c3m.run3        | +2.2              | +2.2         | +0.38                        | +0.58                         | +0.8                       |
| 12 | csiro_mk3_5.20c3m.run1        | +2.8              | +2.1         | +0.44                        | +0.71                         | +1.5                       |
| 13 | csiro_mk3_5.20c3m.run2        | +6.8              | +2.3         | +0.59                        | +0.87                         | +1.4                       |
| 14 | csiro_mk3_5.20c3m.run3        | +3.9              | +2.0         | +0.47                        | +0.64                         | +1.1                       |
| 15 | gfdl_cm2_0.20c3m.run1         | +4.3              | +0.5         | +0.02                        | +0.09                         | -0.7                       |
| 16 | gfdl_cm2_1.20c3m.run2         | +2.6              | +1.6         | +0.21                        | +0.29                         | -0.6                       |
| 17 | giss_aom.20c3m.run1           | +2.5              | -            | +0.35                        | +0.49                         | +0.5                       |
| 18 | giss_aom.20c3m.run2           | +3.7              | -            | +0.27                        | +0.39                         | +0.4                       |
| 19 | giss_model_e_h.20c3m.run1     | +4.7              | -            | -                            | +0.34                         | -0.2                       |
| 20 | giss_model_e_h.20c3m.run2     | +6.0              | -            | -                            | +0.24                         | -0.6                       |
| 21 | giss_model_e_h.20c3m.run3     | +5.2              | -            | -                            | +0.25                         | -0.4                       |
| 22 | giss_model_e_h.20c3m.run4     | +3.4              | -            | -                            | +0.25                         | -0.7                       |
| 23 | giss_model_e_h.20c3m.run5     | +5.9              | -            | -                            | +0.31                         | -0.7                       |
| 24 | giss_model_e_r.20c3m.run1     | -0.1              | +0.9         | +0.13                        | +0.18                         | -0.8                       |
| 25 | giss_model_e_r.20c3m.run2     | +4.9              | +2.9         | +0.13                        | +0.27                         | -0.9                       |
| 26 | giss_model_e_r.20c3m.run3     | +2.3              | +0.1         | +0.12                        | +0.23                         | -1.1                       |
| 27 | giss_model_e_r.20c3m.run4     | -0.1              | -0.2         | +0.22                        | +0.39                         | -0.7                       |
| 28 | giss_model_e_r.20c3m.run5     | +0.9              | +0.8         | +0.20                        | +0.37                         | -0.6                       |
| 29 | giss_model_e_r.20c3m.run6     | +3.2              | +0.1         | +0.15                        | +0.27                         | -0.8                       |
| 30 | giss_model_e_r.20c3m.run7     | +0.6              | -0.0         | +0.15                        | +0.34                         | -0.7                       |
|    |                               |                   |              |                              |                               |                            |

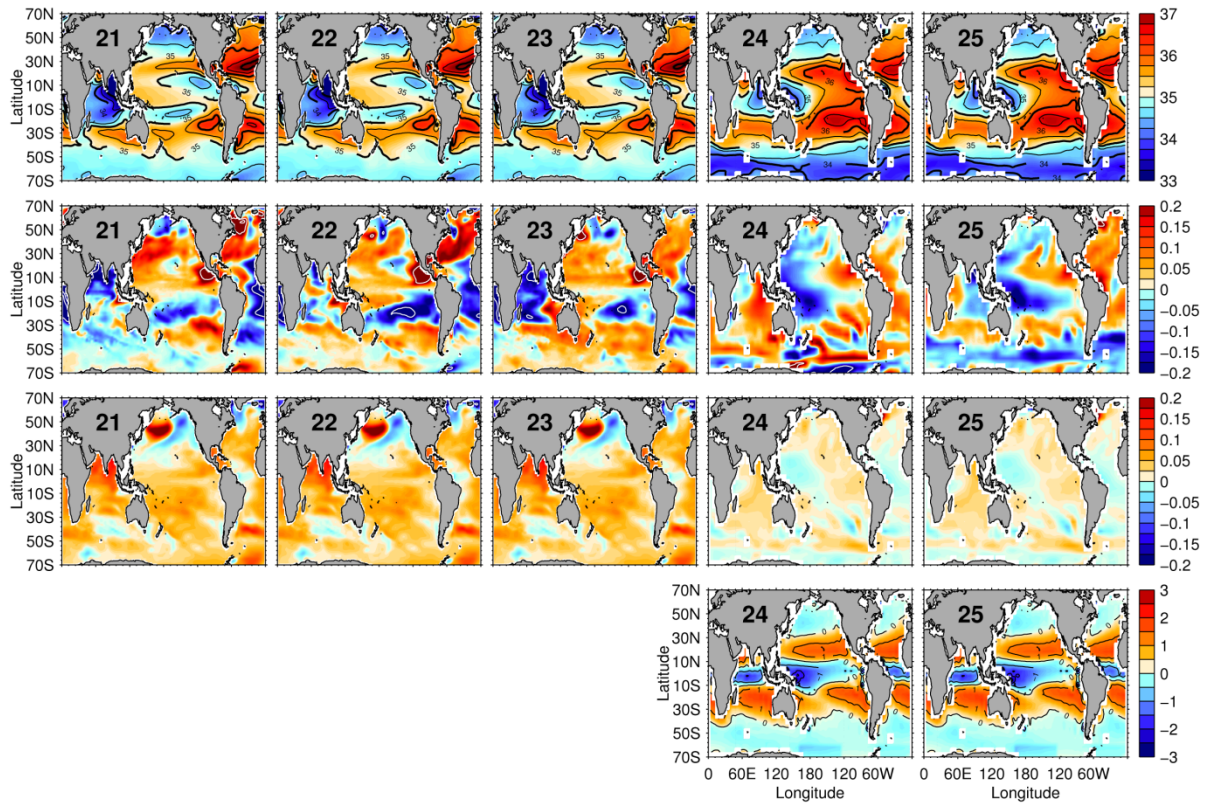
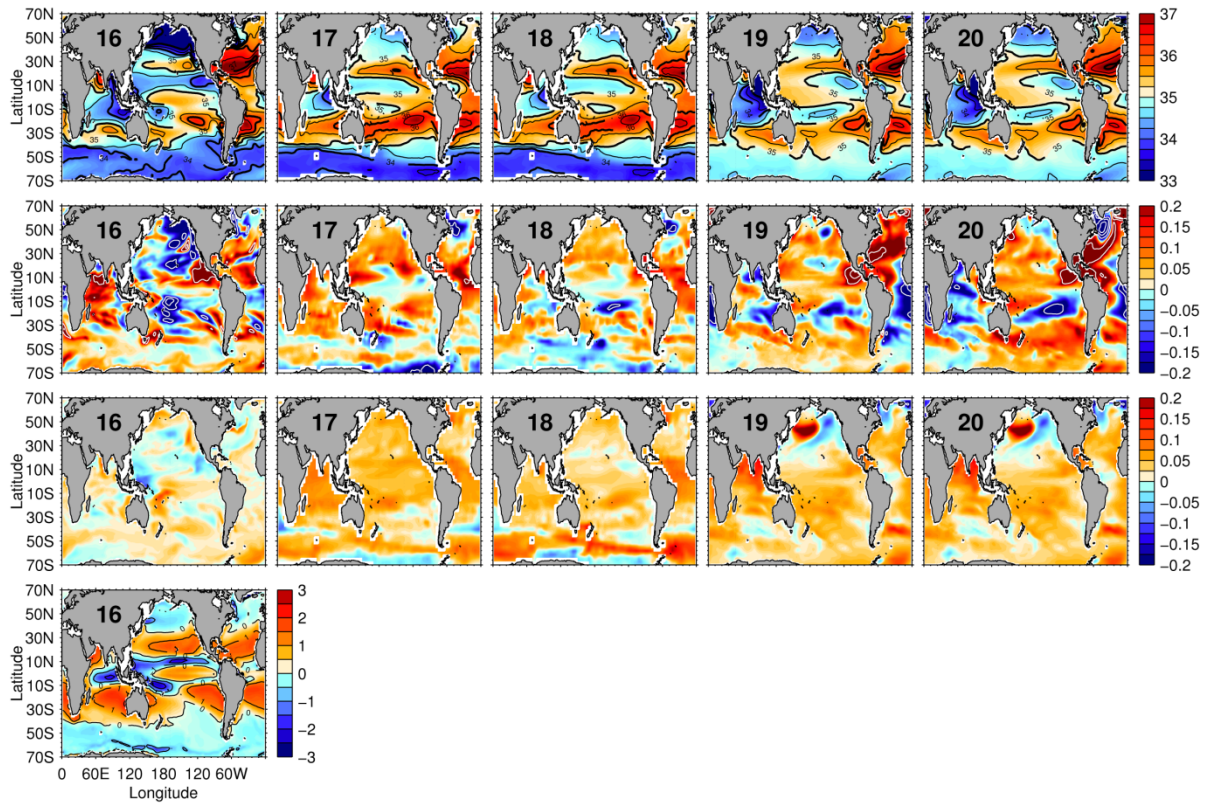
|   | Model                      | Salinity<br>(%PA) | E-P<br>(%PA) | Ocean<br>Temperature<br>(°C) | Global<br>Temperature<br>(°C) | Rainfall<br>(ΔP) |
|---|----------------------------|-------------------|--------------|------------------------------|-------------------------------|------------------|
| 31  | giss_model_e_r.20c3m.run8  | +2.3              | +1.4         | +0.18                        | +0.32                         | -0.8             |
| 32  | giss_model_e_r.20c3m.run9  | +2.7              | +1.5         | +0.13                        | +0.26                         | -0.9             |
| 33  | iap_fgoals1_0_g.20c3m.run1 | +9.4              | +0.5         | +0.48                        | +0.80                         | +0.8             |
| 34  | iap_fgoals1_0_g.20c3m.run2 | +7.5              | -            | -                            | +0.83                         | +1.2             |
| 35  | iap_fgoals1_0_g.20c3m.run3 | +10.2             | -            | -                            | +0.74                         | +0.7             |
| 36  | ingv_echam4.20c3m.run1     | +2.2              | -            | +0.53                        | +0.73                         | +1.4             |
| 37  | ipsl_cm4.20c3m.run1        | +5.4              | -            | +0.42                        | +0.60                         | +0.9             |
| 38  | miroc3_2_hires.20c3m.run1  | +1.7              | -0.4         | +0.37                        | +0.48                         | -0.1             |
| 39  | miroc3_2_medres.20c3m.run1 | +4.8              | +2.3         | +0.16                        | +0.23                         | -0.5             |
| 40  | miub_echo_g.20c3m.run1     | +0.4              | +0.00        | +0.13                        | +0.29                         | -0.3             |
| 41  | miub_echo_g.20c3m.run2     | +4.4              | +2.0         | +0.21                        | +0.32                         | -0.4             |
| 42  | miub_echo_g.20c3m.run3     | +1.0              | +0.2         | +0.16                        | +0.22                         | -0.5             |
| 43  | mpi_echam5.20c3m.run1      | -                 | -            | -                            | +0.48                         | +0.6             |
| 44  | mpi_echam5.20c3m.run2      | -                 | -            | -                            | +0.24                         | -0.2             |
| 45  | mpi_echam5.20c3m.run3      | -                 | -            | -                            | +0.44                         | +0.9             |
| 46  | mri_cgcm2_3_2a.20c3m.run1  | +3.5              | +3.3         | -                            | +0.65                         | +1.1             |
| 47  | mri_cgcm2_3_2a.20c3m.run2  | +1.9              | +3.8         | -                            | +0.62                         | +1.1             |
| 48  | mri_cgcm2_3_2a.20c3m.run3  | +2.0              | +3.3         | -                            | +0.69                         | +1.5             |
| 49  | mri_cgcm2_3_2a.20c3m.run4  | +1.6              | +3.0         | -                            | +0.59                         | +0.8             |
| 50  | mri_cgcm2_3_2a.20c3m.run5  | +4.2              | +4.2         | -                            | +0.63                         | +1.4             |
| 51  | ncar_ccsm3_0.20c3m.run1    | -                 | -            | -                            | +0.32                         | -0.2             |
| 52  | ncar_ccsm3_0.20c3m.run3    | -                 | -            | -                            | +0.52                         | +0.2             |
| 53  | ncar_pcm1.20c3m.run1       | -                 | -            | -                            | -                             | -                |
| 54  | ncar_pcm1.20c3m.run3       | -                 | -            | -                            | -                             | -                |
| 55  | ncar_pcm1.20c3m.run4       | -                 | -            | -                            | -                             | -                |
| 56  | ukmo_hadcm3.20c3m.run1     | +0.1              | +1.7         | -                            | +0.60                         | +0.5             |
| 57  | ukmo_hadcm3.20c3m.run2     | +4.7              | +4.3         | -                            | +0.67                         | +0.3             |
| 58  | ukmo_hadgem1.20c3m.run1    | +1.1              | +1.3         | +0.40                        | +0.60                         | +0.2             |
| 20C3M Models                                |                            | 20                | 16           | 16                           | 23                            | 23               |
| 20C3M Simulations                           |                            | 58                | 47           | 63                           | 78                            | 73               |
| 20C3M De-drifted Simulations                |                            | 50                | 44           | 41                           | 70                            | 68               |
| Ensemble Mean                               |                            | +3.7              | +2.0         | +0.33                        | +0.50                         | +0.3             |
| Ensemble Standard Deviation                 |                            | +2.4              | +1.8         | +0.20                        | +0.25                         | +0.9             |
| Observational Estimates                     |                            | Salinity<br>(%PA) | E-P<br>(%PA) | Ocean<br>Temperature<br>(°C) | Global<br>Temperature<br>(°C) | Rainfall<br>(ΔP) |
| Durack & Wijffels (2010; 1950-2000)         |                            | +8.0              |              | +0.49                        |                               |                  |
| Boyer <i>et al.</i> (2005; 1955-1998)       |                            | +5.4              |              |                              |                               |                  |
| Wijffels <i>et al.</i> (in prep; 1960-2008) |                            |                   |              | +0.56                        |                               |                  |
| HadCRUT3 (1950-2009)                        |                            |                   |              |                              | +0.54                         |                  |
| GISTEMP (1950-2009)                         |                            |                   |              |                              | +0.53                         |                  |
| Levitus <i>et al.</i> (2009; 1955-2009)     |                            |                   |              | +0.25                        |                               |                  |
| HadSST2 (1950-2009)                         |                            |                   |              | +0.37                        |                               |                  |
| HadSST3 (1950-2006)                         |                            |                   |              | +0.27                        |                               |                  |
| Kaplan V2 (1950-2009)                       |                            |                   |              | +0.24                        |                               |                  |
| ERSST V3b (1950-2009)                       |                            |                   |              | +0.31                        |                               |                  |
| OAFlux V3 (1958-2008)                       |                            |                   | +6.4         |                              |                               |                  |
| GPCP V2.1 (1979-2008)                       |                            |                   |              |                              |                               | -3.7             |
| GPCP V2.2 (1979-2010)                       |                            |                   |              |                              |                               | -4.7             |
| CMAP (1979-2008)                            |                            |                   |              |                              |                               | -6.0             |

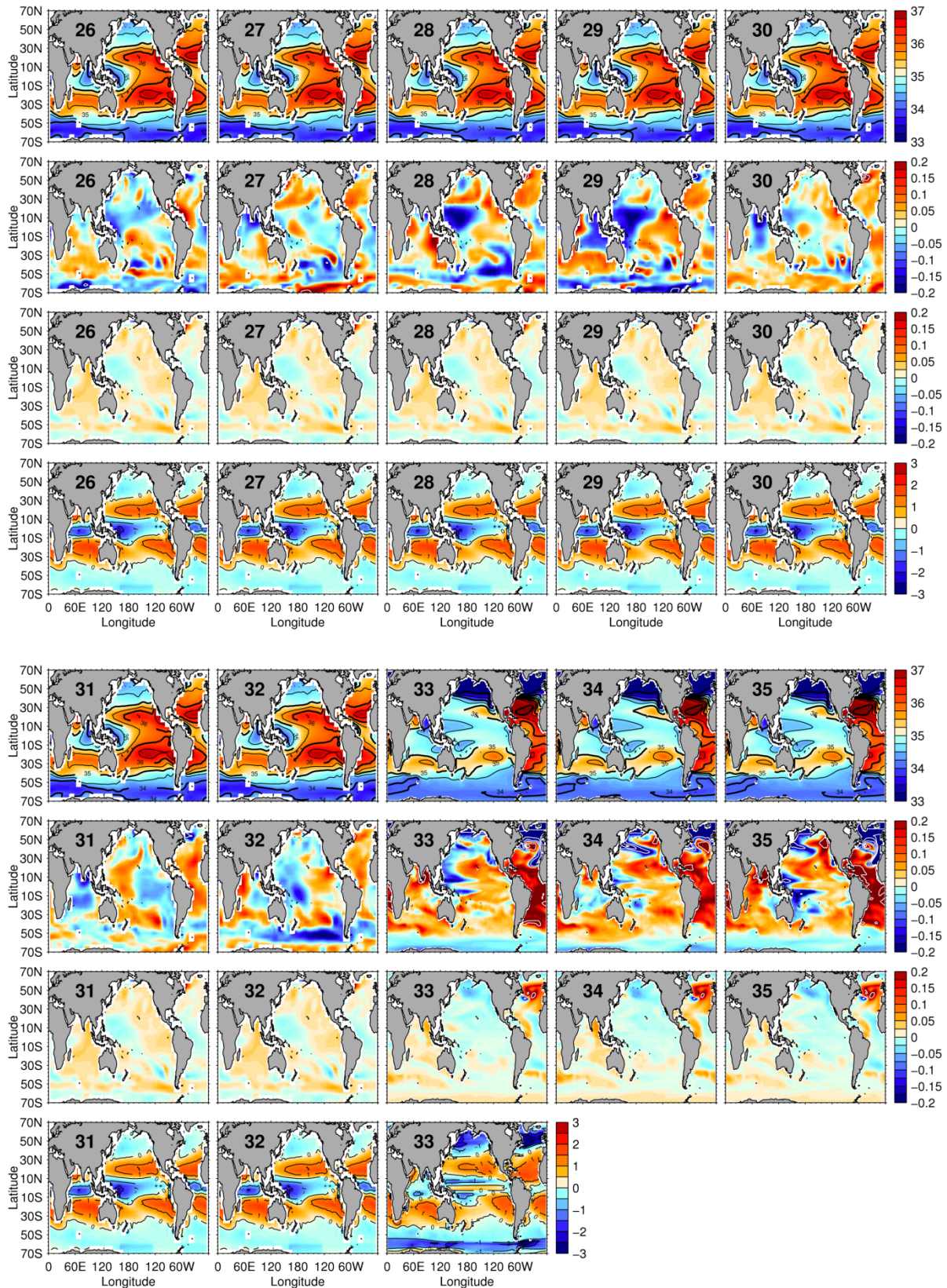
In order to present the full range of CMIP3 20C3M spatial salinity responses, each of the 58 available model salinity patterns are expressed in Figure S6. These panels show the 1950-2000 mean salinity (top row), the 1950-2000 linear trend ( $2^{\text{nd}}$  row), the corresponding drift, as captured by a linear trend from the corresponding preindustrial control (PICNTRL) over the years 1900-2049 ( $3^{\text{rd}}$  row), and the 1950-2000 mean E-P (bottom row).

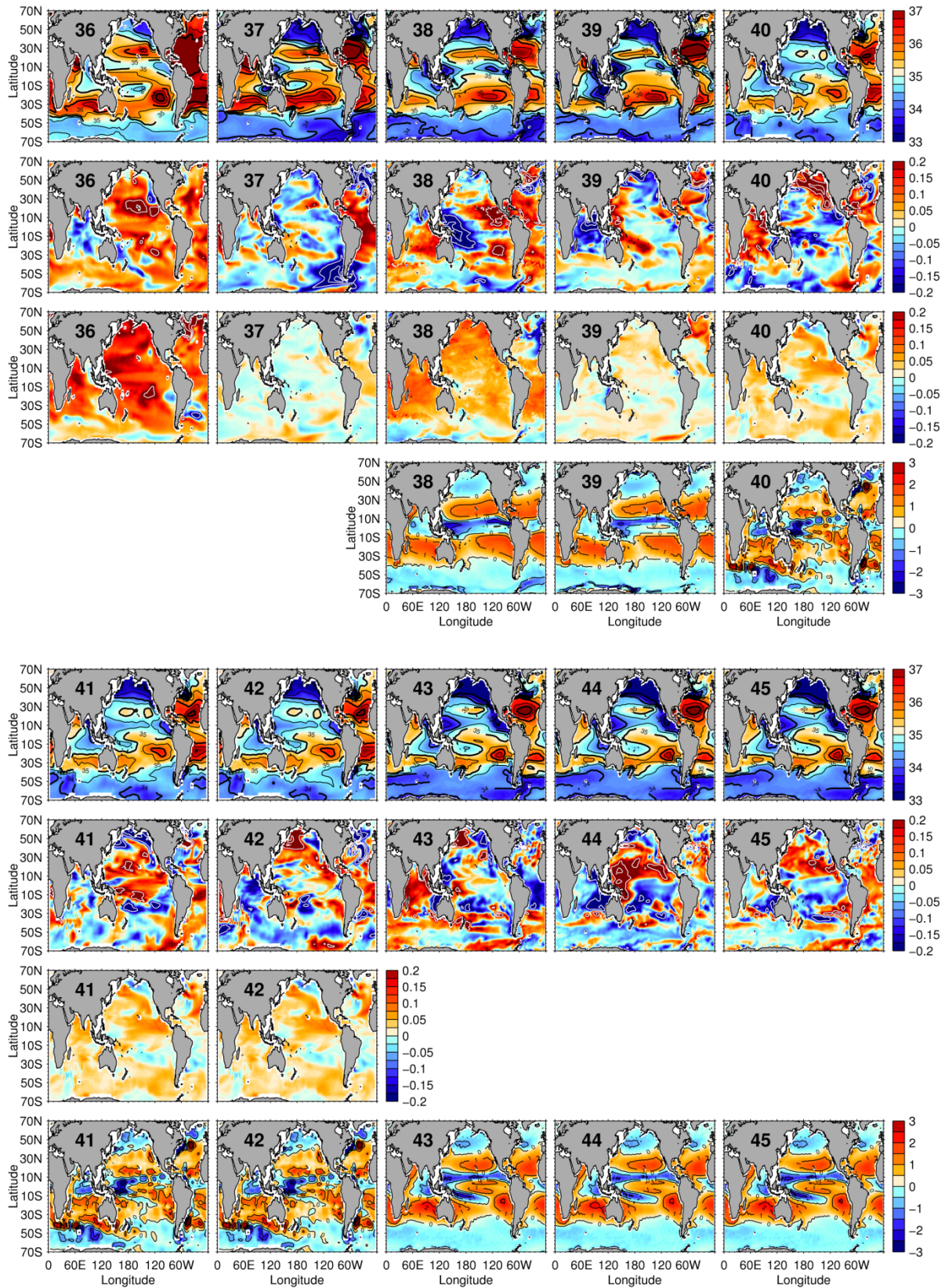
Figure S6. Ocean salinity amplification is expressed by 23 CMIP3 global climate models in their 20C3M simulations for the period 1950-2000. Top vertical panel represents climatological annual mean surface salinity for 1950-2000, second vertical panel represents 20C3M surface salinity change for 1950-2000, third vertical panel represents the corresponding PICNTRL drift as determined for 1900-2049 and the lowest vertical panel represents climatological annual mean surface water flux (E-P) for 1950-2000. Panel numbers represent each model/simulation as numbered in Table S2.

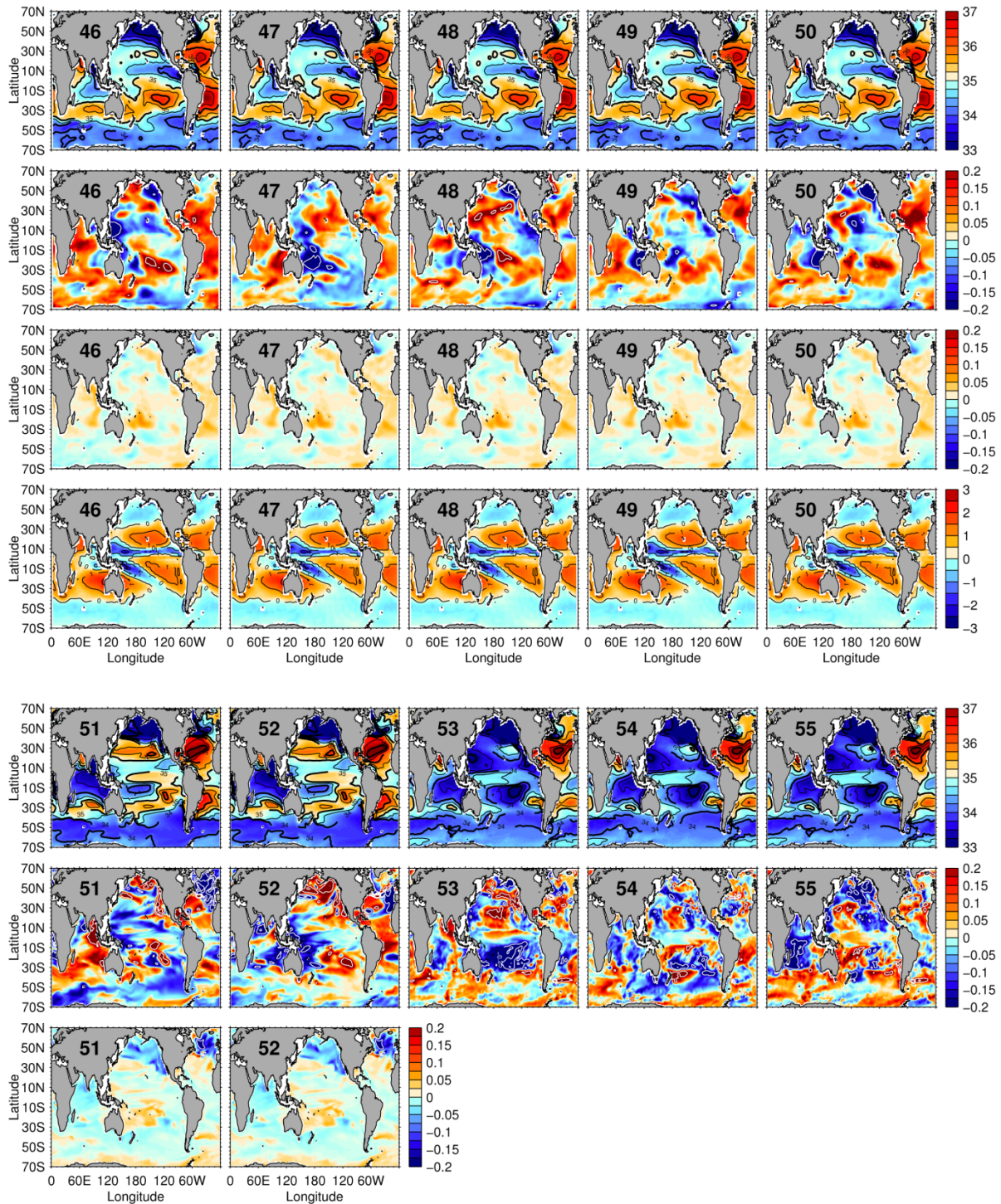


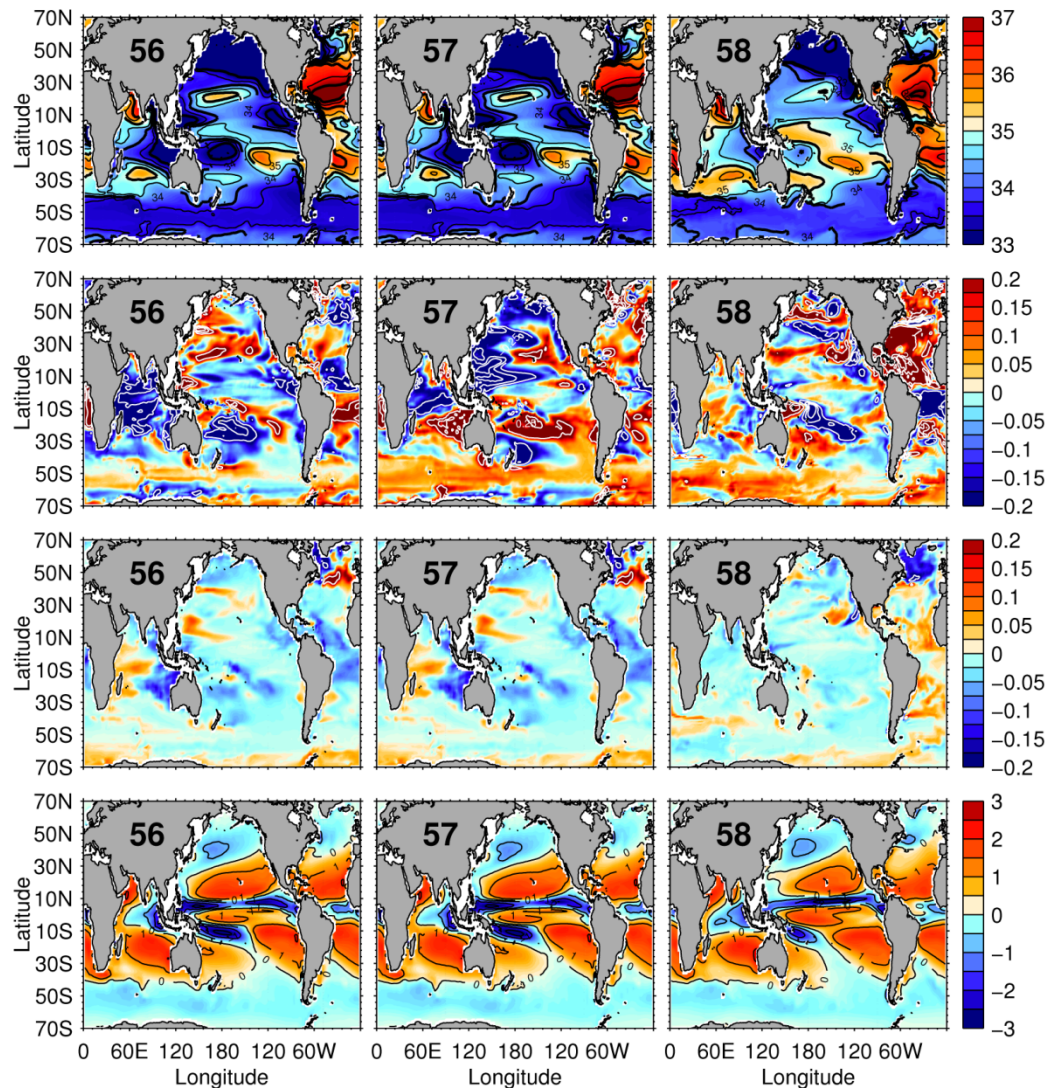












### **3. Idealised Ocean-model Experiments**

A version of the MOM3 ocean model (41), forced with surface water flux fields obtained from the NCEP reanalysis was used in this analysis. These experiments were constructed to test the salinity response to an idealised, linearly increasing E-P forcing over an equivalent time period to the observational salinity analysis (1950-2000). The model was spun-up over the representative years 1850 to 1948 with daily surface fluxes. The ocean was initialised using the climatological fields of temperature and salinity from the World Ocean Atlas 2001 (42). In order to minimise modelled climate variability and enhance the spatial change signal in the idealised runs, a single year (1948) from the NCEP-1 reanalysis (43) was selected. This data then provided the daily surface forcing fields; wind stresses, heat and water fluxes, which were perennially applied to the ocean model. These 1948 annual fluxes were then used for the model spin-up, 1850-1948 with both sea surface temperature (SST; 44) and salinity (42) restored to annual climatologies on a 30 day timescale. For the idealised runs, and the corresponding control run (which extended from 1948-2009), salinity restoring was not undertaken, however SST restoring was enabled. In plots presented in Figure S7 and S8 we show the salinity change with the control run drift removed, with the difference attributable to the idealised surface E-P forcing.

Linear increasing trends to surface water fluxes were imposed over the 1948-2009 period. To attempt to capture the range of linear and non-linear responses to such surface water flux changes, runs imposed with a 5%, 10%, 15% and 20% E-P change were undertaken, additional to a control with no changes to surface water fluxes. These model runs were then investigated for their surface (and subsurface) salinity changes, and compared to the comparative 1950-2000 observed patterns of salinity change.

Each of the model runs (Figure S7, C, D, E and F) expresses the surface salinity response for the 50 year period over which the linear increasing trend to E-P was imposed, with the corresponding control drift removed point-wise from each representative field. These idealised runs tend to replicate the broad-scale patterns of the observational analysis (Figure S7A). A coherent freshening of the Pacific is apparent, with the exception of a zonal enhancement to surface salinities located along the subtropical salinity maxima, broadly following the E-P maxima of the basin. In the Atlantic, strong surface salinity increases are apparent aligned with the subtropical salinity maxima in both the North and South Atlantic. In the Indian, an enhanced salinity is found in the Arabian Sea, with a strong freshening in the Bay of Bengal. The enhanced salinity, associated with the subtropical salinity maxima is much broader in observations when compared to the idealised model results.

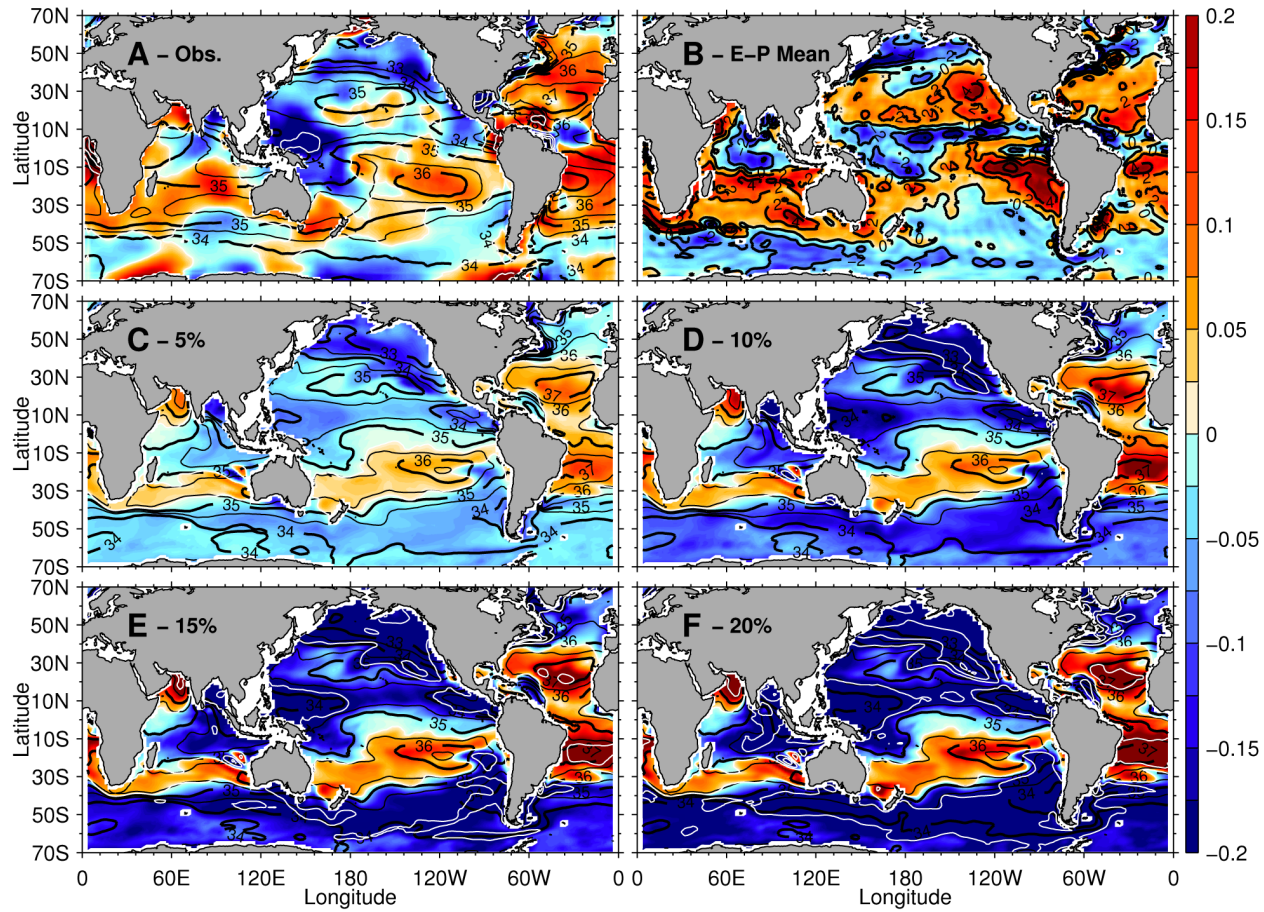


Figure S7. Patterns of 50 year surface salinity change (PSS-78 50 year<sup>-1</sup>). A) The 1950-2000 observational result of (25). B) The climatological annual mean surface water flux (m year<sup>-1</sup>) as obtained from NCEP-1 (43). The idealised surface salinity response for a: C) 5%, D) 10%, E) 15% and F) 20% surface water flux enhancement over 50 years. For each panel, the corresponding mean salinity is contoured in black, with thick lines every 1 (PSS-78) and thin lines every 0.5 (PSS-78).

Additional to a surface salinity comparison, global subsurface zonal mean comparison was also undertaken (Figure S8). A strong coherence was found between the observed result (Figure S8A) and those of the idealised simulations. In these simulations the salty southern subtropical gyre bowl is expressing a strong enhanced salinity, whereas the Northern Hemisphere response is less coherent. The high latitude freshening is also captured in this model, however the subduction of this signal into the ocean interior is weaker than in observations, particularly in the Southern Hemisphere. This feature is most clear when comparing the climatological salinity (contoured) with a deep and clear salinity minima tongue visible extending to 1500 dbar in observations (Figure S8A), with this feature noticeably absent in the model (Figure S8B-E). The independent basin changes (not shown) provide even stronger evidence that regional basin-wide salinity changes, reported in observations are linked to E-P changes at the surface. We note that this model does not provide a perfect replication of the global ocean structure, with a weaker salinity minima subduction and circulation pathway into the deep interior when compared to our observational understanding (contrast Figure S8, A versus B, C, D and E). This could then lead to difficulties in interpreting deeper ocean changes on longer timescales ( $> 50$  years) as the model replication of such deep ocean interior changes are likely to be smaller in magnitude when compared to observations.

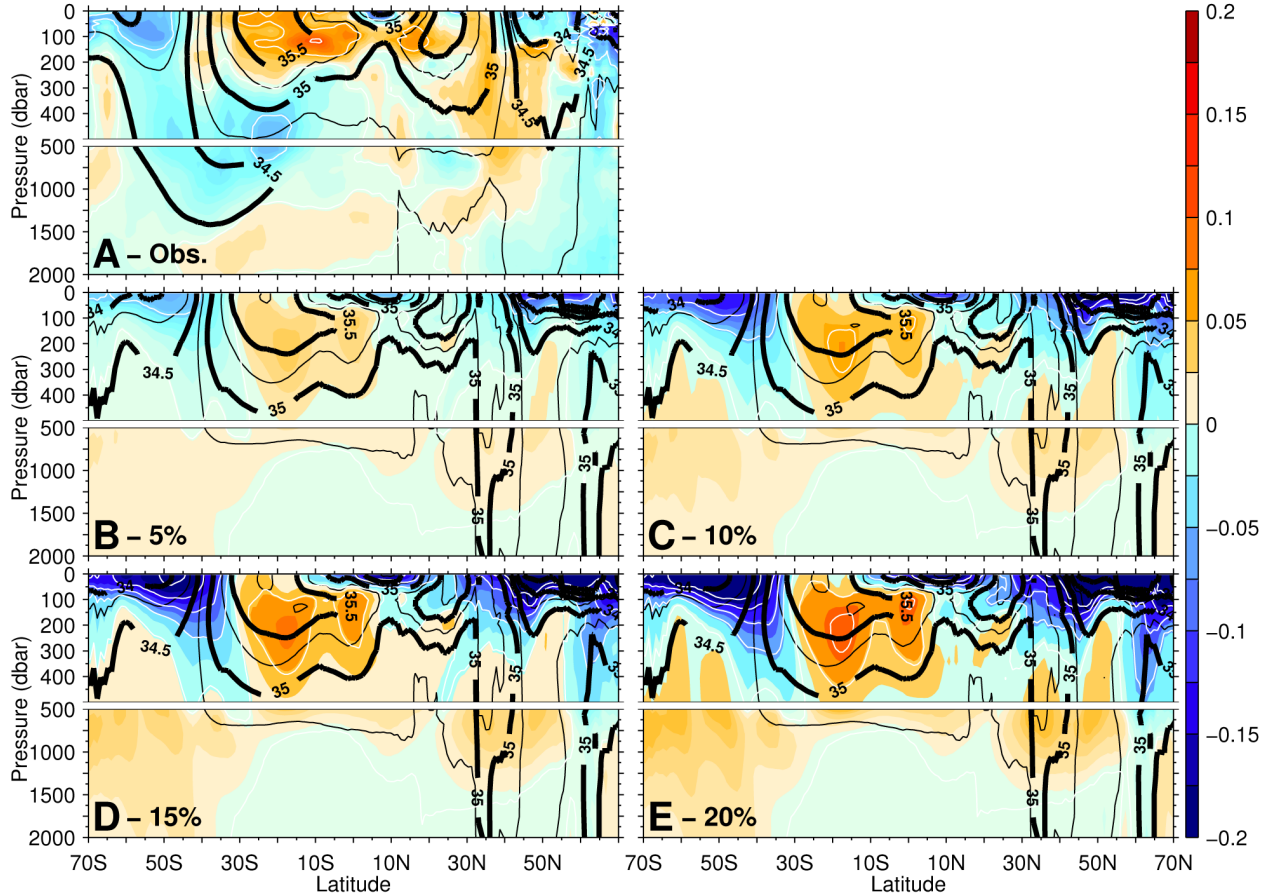


Figure S8. Patterns of 50 year subsurface zonal mean salinity change ( $\text{PSS-78 } 50 \text{ year}^{-1}$ ). A) The 1950-2000 observational result of (25). The idealised subsurface salinity response for a: B) 5%, C) 10%, D) 15% and E) 20% surface water flux enhancement over 50 years. For each panel, the corresponding mean salinity is contoured in black, with thick lines every 0.5 (PSS-78) and thin lines every 0.25 (PSS-78).

When comparing these idealised model simulations to those of the CMIP3 suite it is clear that this ocean-only simulation underestimates the CMIP3 1:2 relationship between E-P and SSS PA (not shown, with a value near 1:1). Three reasons for these differences may include:

- 1) A link between ocean warming and the SSS trend which amplifies the resolved SSS PA
- 2) Net sea-ice melt in the CMIP3 simulations provides an additional freshwater source term which is not included in the idealised ocean-only simulations
- 3) Terrestrial storage changes in CMIP3 (not captured by idealised simulations) influences the 1:2 relationship between E-P and SSS PA

Some preliminary investigations suggest that ocean warming when coupled with the idealised E-P forcing does increase the SSS PA – this is possibly linked to increasing ocean stratification, where a smaller control volume is experiencing the effects of the E-P forcing. Some CMIP3 analyses (45, 46, 47) suggest such stratification changes will occur due to climate change, however, dynamically these changes are complex (45). Changes to terrestrial E-P and the resulting runoff is another potential source of ocean change with more regional effects likely, however such effects are not captured in the idealised ocean-only simulations. The reduction in

summer sea-ice in CMIP3 projections, particularly in the Arctic (48, 49) could also drive strong change, with large SSS declines in the high latitudes suggesting this process may be operating – we note again however that dynamic ice processes are not included in these idealised ocean-only simulations.

The lack of these 3 processes in the idealised ocean-only simulations makes the CMIP3 simulations a better choice in which to calibrate the E-P PA and SSS PA.

#### **4. Observational Estimates of Water Cycle Change**

Estimates of water cycle change have been obtained from numerous observational and satellite-based platforms. How do resolved changes from differing observed platforms compare to the new water cycle change estimate expressed by ocean salinity from 1950-2000? In Figure S9 and Table S3 we compile a non-exhaustive list of observed water cycle change estimates from many selected studies, with each of these expressing the explicit rate of water cycle rate per degree of global surface warming over the corresponding period of analysis, obtained from HadCRUT3 (50).

It is clear when reviewing the comparative results presented in Figure S8 that a large portion of these observed estimates suggests that a water cycle response on or near Clausius-Clapeyron ( $7\% \text{ }^{\circ}\text{C}^{-1}$ ). It is also clear that no matter which CMIP3 ensemble mean estimate is utilised (salinity, E-P or global mean rainfall), these tend to provide conservative estimates of such changes when compared to the available observational comparisons.

Many of the presented atmospheric estimates provide trends obtained over periods less than 30 years, and so decadal climate variability may strongly influence such short-term trends. Additionally, the use of satellite data from numerous independent missions ensures that difficulties with cross-mission calibration can strongly influence the magnitude and sign of the resolved trends (see main text).

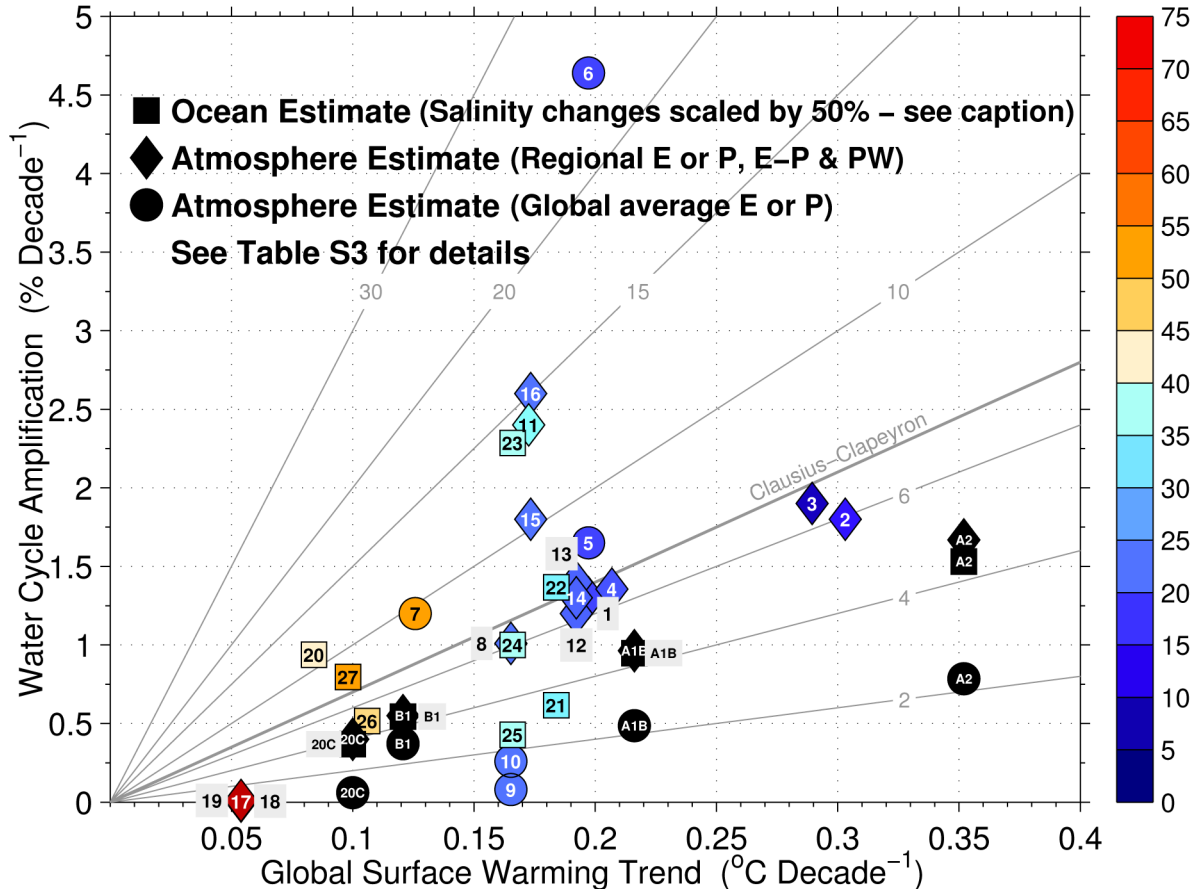


Figure S9. Reported observed water cycle changes (scaled in relative absolute change decade $^{-1}$ ). Colors indicate years over which reported changes are calculated (red is longer). As noted in the figure, ocean salinity estimates are presented as squares (scaled by 50% of their reported salinity change magnitudes to represent equivalent E-P change as obtained from the CMIP3 ensemble relationship, see text), atmospheric water cycling estimates (non-average global rainfall/evaporation) are triangles and average global rainfall/evaporation are circles. All  $\Delta T_a$  trends were obtained from HadCRUT3 (50) using a linear fit over the corresponding years (annual data) used to determine the water cycle change estimate. More detail, including error estimates for each of the noted studies is contained in Table S3. The result suggested by this study is #27. For reference, equivalent scenario ensemble mean changes for the 20C3M (1950-2000; 20C) and SRES (2050-2099; B1, A1B, A2) simulations are included in black. Gray lines express constant proportional change; line representing Clausius-Clapeyron (CC) is 7%  $^{\circ}\text{C}^{-1}$ . A total of 16 independent studies and 27 estimates of global and regional changes which express different aspects of regional or global water cycle change are presented.

Table S3: Some representative observed water cycle changes for the 20<sup>th</sup> and early 21<sup>st</sup> century, as expressed in Figure S9. Salinity (not published inferred E-P) estimates are scaled by 50% (in Figure S9 – numbers 20 through 27 below; unscaled salinity values are tabulated below) to represent E-P changes using the relationship obtained from the CMIP3 model suite (see main text). All global warming trends were obtained from HadCRUT3 (50) as a linear trend over the period of analysis, following the MetOffice smoothed annual average temperature technique described at <http://hadobs.metoffice.com/hadcrut3/smoothing.html> (accessed 11th April 2012). Error estimates in the last column indicate formal errors resolved from the linear warming trend combined with water cycle error bounds (if available). Estimates are presented at 99% confidence for the warming plus the water cycle error (if provided).

|    | Author                          | Instrument         | Region  | Period    | Change per Decade | Change per K           |
|----|---------------------------------|--------------------|---|-----------|-------------------|------------------------|
| 1  | Trenberth <i>et al.</i> , 2005  | SSM/I              | Global PW over Oceans                                   | 1987-2004 | 1.3±0.3%          | 7±16% K <sup>-1</sup>  |
| 2  | Keihm <i>et al.</i> , 2009      | TMR                | Global PW 60°S-60°N                                     | 1992-2005 | 1.8±0.4%          | 6±9% K <sup>-1</sup>   |
| 3  | Mieruch <i>et al.</i> , 2008    | GOME & SCIAMACHY   | Global PW   | 1996-2002 | 1.9±0.7%          | 7±4% K <sup>-1</sup>   |
| 4  | Santer <i>et al.</i> , 2007     | SSM/I              | Global PW over Oceans 50°S-50°N                         | 1988-2006 | 1.4±0.7%          | 7±14% K <sup>-1</sup>  |
| 5  | Liepert & Previdi, 2009         | OAFlux             | Global Ocean E  | 1987-2004 | 1.6±0.8%          | 8±27% K <sup>-1</sup>  |
| 6  | Liepert & Previdi, 2009         | HOAPS              | Global Ocean E  | 1987-2004 | 4.6±3.6%          | 24±95% K <sup>-1</sup> |
| 7  | Yu, 2007 (updated, pers. Comm.) | OAFlux_V3          | Global Ocean E  | 1958-2008 | 1.2±0.5%          | 10±8% K <sup>-1</sup>  |
| 8  | Li <i>et al.</i> , 2011         | SSM/I              | Global PW over Oceans                                   | 1988-2009 | 1.0±0.4%          | 6±14% K <sup>-1</sup>  |
| 9  | Li <i>et al.</i> , 2011         | SSM/I              | Global Ocean P  | 1988-2009 | 0.1±0.4%          | 0±7% K <sup>-1</sup>   |
| 10 | Li <i>et al.</i> , 2011         | GPCP_V2.1SSM/I     | Global Surface P  | 1988-2009 | 0.3±0.4%          | 2±8% K <sup>-1</sup>   |
| 11 | Durre <i>et al.</i> , 2009      | Radiosondes        | Northern Hemisphere PW                                  | 1973-2006 | 2.4%              | 14% K <sup>-1</sup>    |
| 12 | Wentz <i>et al.</i> , 2007      | SSM/I              | Tropical PW   | 1987-2006 | 1.2±0.4%          | 6±11% K <sup>-1</sup>  |
| 13 | Wentz <i>et al.</i> , 2007      | SSM/I              | Tropical P  | 1987-2006 | 1.4±0.5%          | 7±14% K <sup>-1</sup>  |
| 14 | Wentz <i>et al.</i> , 2007      | SSM/I              | Tropical E  | 1987-2006 | 1.3±0.5%          | 7±13% K <sup>-1</sup>  |
| 15 | Allan <i>et al.</i> , 2010      | GPCP_V2.1/SSM/I    | Tropical Hi-P   | 1988-2008 | 1.8±0.5%          | 10±23% K <sup>-1</sup> |
| 16 | Allan <i>et al.</i> , 2010      | GPCP_V2.1/SSM/I    | Tropical Lo-P   | 1988-2008 | -2.6±0.8%         | -15±9% K <sup>-1</sup> |
| 17 | Zhang <i>et al.</i> , 2007      | GHCN               | Land P 30°S-0   | 1925-1999 | 0.006%            | <1% K <sup>-1</sup>    |
| 18 | Zhang <i>et al.</i> , 2007      | GHCN               | Land P 0-30°N   | 1925-1999 | -0.007%           | <1% K <sup>-1</sup>    |
| 19 | Zhang <i>et al.</i> , 2007      | GHCN               | Land P 40-70°N  | 1925-1999 | 0.01%             | <1% K <sup>-1</sup>    |
| 20 | Curry <i>et al.</i> , 2003      | Ocean profile data | E-P inferred (Atlantic salinity)                        | 1950-1990 | 1.9% (5-10)       | 22% K <sup>-1</sup>    |
| 21 | Hosoda <i>et al.</i> , 2009     | Ocean profile data | E-P inferred (Global salinity)                          | 1974-2005 | 1.2±1.5%          | 7±14% K <sup>-1</sup>  |
| 22 | Hosoda <i>et al.</i> , 2009     | Ocean profile data | E-P inferred (Southern Ocean salinity)                  | 1974-2005 | 2.7±2.1%          | 15±22% K <sup>-1</sup> |
| 23 | Helm <i>et al.</i> , 2010       | Ocean profile data | E-P inferred (Southern Ocean salinity)                  | 1970-2005 | 4.6±1.7%          | 28±25% K <sup>-1</sup> |
| 24 | Helm <i>et al.</i> , 2010       | Ocean profile data | E-P inferred (Northern Hemisphere Hi-latitude salinity) | 1970-2005 | 2.0±1.1%          | 12±14% K <sup>-1</sup> |
| 25 | Helm <i>et al.</i> , 2010       | Ocean profile data | E-P inferred (Subtropical gyres salinity)               | 1970-2005 | -0.9±0.6%         | -5±4% K <sup>-1</sup>  |
| 26 | Boyer <i>et al.</i> , 2005      | Ocean profile data | Global Ocean surface salinity                           | 1955-1998 | 1.0±0.1%          | 10±7% K <sup>-1</sup>  |
| 27 | This study                      | Ocean profile data | Global Ocean surface salinity                           | 1950-2000 | 1.6±0.2%          | 16±10% K <sup>-1</sup> |
| -  | This study                      | Ocean profile data | Pacific Ocean surface salinity                          | 1950-2000 | 1.4±0.1%          | 15±7% K <sup>-1</sup>  |
| -  | This study                      | Ocean profile data | Atlantic Ocean surface salinity                         | 1950-2000 | 1.4±0.1%          | 15±7% K <sup>-1</sup>  |
| -  | This study                      | Ocean profile data | Indian Ocean surface salinity                           | 1950-2000 | 1.2±0.1%          | 12±7% K <sup>-1</sup>  |

## References and Notes

33. Baumgartner, A. and E. Reichel (1975) The World Water Balance: Mean Annual Global, Continental and Maritime Precipitation, Evaporation and Runoff. Elsevier Science Ltd. Amsterdam. 179 pp
34. Schmitt, R.W. (1995) The ocean component of the global water cycle. *Reviews of Geophysics*, 33 (Supplement; U.S. National Report to the International Union of Geodesy and Geophysics, 1991-1994), pp 1395-1409
35. Trenberth, K.E., L. Smith, T. Qian, A. Dai and J. Fasullo (2007) Estimates of the Global Water Budget and Its Annual Cycle Using Observational and Model Data. *Journal of Hydrometeorology*, 8, pp 758-769. doi: 10.1175/jhm600.1
36. Steffen, K., R.H. Thomas, E. Rignot, J.G. Cogley, M.B. Dyurgerov, S.C.B. Raper, P. Huybrechts and E. Hanna (2010) Cryospheric Contributions to Sea-Level Rise and Variability. In *Understanding Sea-Level Rise and Variability*, Church, J.A., P.L. Woodworth, T. Aarup and W.S. Wilson (Eds) Wiley-Blackwell, Oxford, U.K. pp 178-225. doi: 10.1002/9781444323276
37. Sen Gupta, A., L.C. Muir, J.N. Brown, S.J. Phipps, P.J. Durack, D. Monselesan and S.E. Wijffels (2012) Climate Drift in the CMIP3 Models. *Journal of Climate*, Early Online Release. doi: 10.1175/JCLI-D-11-00312.1
38. Chen, G., Y. Ming, N.D. Singer and J. Lu (2011) Testing the Clausius-Clapeyron constraint on the aerosol-induced changes in mean and extreme precipitation. *Geophysical Research Letters*, 38, L04807. doi: 10.1029/2010GL046435
39. Santer, B.D., C. Mears, F.J. Wentz, K.E. Taylor, P.J. Gleckler, T.M.L. Wigley, T.P. Barnett, J.S. Boyle, W. Bruggemann, N.P. Gillett, S.A. Klein, G.A. Meehl, T. Nozawa, D.W. Pierce, P.A. Stott, W.M Washington and M.F. Wehner (2007) Identification of human-induced changes in atmospheric moisture content. *Proceedings of the National Academy of Sciences*, 104, pp 15248-15253. doi: 10.1073/pnas.0702872104
40. Levitus, S., J.I. Antonov, T.P. Boyer, R.A. Locarnini, H.E. Garcia and A.V Mishonov (2009) Global ocean heat content 1955-2008 in light of recently revealed instrumentation problems. *Geophysical Research Letters*, 36, L070608. doi: 10.1029/2008GL037155
41. Matear, R.J. and A. Lenton (2008) Impact of Historical Climate Change on the Southern Ocean Carbon Cycle. *Journal of Climate*, 21, pp 5820-5834. doi: 10.1175/2008JCLI2194.1
42. Conkright, M.E., R.A. Locarnini, H.E. Garcia, T.D. O'Brien, T.P. Boyer, C. Stephens and J.I. Antonov (2002) World Ocean Atlas 2001: Objective Analyses, Data Statistics and Figures. NODC Internal Report 17, 17 pp
43. Kalnay, E., M. Kanamitsu, R. Kistler, W. Collins, D. Deaven, L. Gandin, M. Iredell, S. Saha, G. White, J. Woollen, Y. Zhu, A. Leetmaa and R. Reynolds (1996) The NCEP/NCAR 40-Year Reanalysis Project. *Bulletin of the American Meteorological Society*, 77, pp 437-473. doi: 10.1175/1520-0477(1996)077<0437:TNYRP>2.0.CO;2
44. Reynolds, R.W. and T.M. Smith (1994) Improved Global Sea Surface Temperature Analyses Using Optimal Interpolation. *Journal of Climate*, 7, pp 929-948. doi: 10.1175/1520-0442(1994)007<0929:IGSSTA>2.0.CO;2
45. Russell, J.L., K.W. Dixon, A. Gnanadesikan, R.J. Stouffer and J.R. Toggweiler (2006) The Southern Hemisphere Westerlies in a Warming World: Propping Open the Door to the Deep Ocean. *Journal of Climate*, 19, pp 6382-6390. doi: 10.1175/JCLI3984.1

46. Luo, Y., Q. Liu ad L.M. Rothstein (2009) Simulated response of North Pacific Mode Waters to global warming. *Geophysical Research Letters*, 36, L23609. doi: 10.1029/2009GL040906
47. Jang, C.J., J. Park, T. Park and S. Yoo (2011) Response of the ocean mixed layer depth to global warming and its impact on primary production: a case for the North Pacific Ocean. *ICES Journal of Marine Science*, 68, pp 996-1007. doi: 10.1093/icesjms/fsr064
48. Zhang, X. and J.E. Walsh (2006) Toward a Seasonally Ice-Covered Arctic Ocean: Scenarios from the IPCC AR4 Model Simulations. *Journal of Climate*, 19, pp 1730-1747. doi: 10.1175/JCLI3767.1
49. Wang, M. and J.E. Overland (2009) A sea ice free summer Arctic within 30 years? *Geophysical Research Letters*, 36, L07502. doi: 10.1029/2009GL037820
50. Brohan, P., J.J. Kennedy, I. Harris, S.F.B. Tett and P.D. Jones (2006) Uncertainty estimates in regional and global observed temperature changes: A new data set from 1850. *Journal of Geophysical Research*, 111, D12106. doi: 10.1029/2005JD006548
51. Trenberth, K.E., J. Fasullo and L. Smith (2005) Trends and variability in column-integrated atmospheric water vapor. *Climate Dynamics*, 24, pp 741-758. doi: 10.1007/s00382-005-0017-4
52. Keihm, S., S. Brown, J. Teixeira, S. Desai, W. Lu, E. Fetzer, C. Ruf, X. Huang and Y. Yung (2009) Ocean water vapor and cloud liquid water trends from 1992 to 2005 TOPEX Microwave Radiometer data. *Journal of Geophysical Research*, 114, D18101. doi: 10.1029/2009JD012145
53. Mieruch, S., S. Noël, H. Bovensmann and J.P. Burrows (2008) Analysis of global water vapour trends from satellite measurements in the visible spectral range. *Atmospheric Chemistry and Physics*, 8, pp 491-504. doi: 10.5194/acp-8-491-2008
54. Liepert, B.G. and M. Previdi (2009) Do Models and Observations Disagree on the Rainfall Response to Global Warming? *Journal of Climate*, 22, pp 3156-3166. doi: 10.1175/2008JCLI2472.1
55. Yu, L. (2007) Global Variations in Oceanic Evaporation (1958-2005): The Role of the Changing Wind Speed. *Journal of Climate*, 20, pp 5376-5390. doi: 10.1175/2007JCLI1714.1
56. Li, L., X. Jiang, M.T. Chahine, E.T. Olsen, E.J. Fetzer, L. Chen and Y.L. Yung (2011) The recycling rate of atmospheric moisture over the past two decades (1988-2009). *Environmental Research Letters*, 6, 034018. doi: 10.1088/1748-9326/6/3/034018
57. Durre, I., C.N. Williams Jr, X. Yin and R.S. Vose (2009) Radiosonde-based trends in precipitable water over the Northern Hemisphere: An update. *Journal of Geophysical Research*, 114, D05112. doi: 10.1029/2008JD010989
58. Allan, R.P., B.J. Soden, V.O. John, W. Ingram and P. Good (2010) Current changes in tropical precipitation. *Environmental Research Letters*, 5, 025205. doi: 10.1088/1748-9326/5/2/025205
59. Zhang, X., F.W. Zwiers, G.C. Hegerl, F.H. Lambert, N.P. Gillett, S. Solomon, P.A. Stott and T. Nozawa (2007) Detection of human influence on twentieth-century precipitation trends. *Nature*, 448, pp 461-465. doi: 10.1038/nature06025
60. Curry, R., B. Dickson and I. Yashayaev (2003) A change in the freshwater balance of the Atlantic Ocean over the past four decades. *Nature*, 426, pp 826-829. doi: 10.1038/nature02206